MASS TRANSFER MODELING OF DRI PARTICLE-SLAG HEAT TRANSFER IN THE ELECTRIC FURNACE

by

RANDALL STEPHEN WRIGHT

B.Mech.E. University of Minnesota
1977

Submitted in partial fulfillment of the requirements

for the degree of

MASTER OF SCIENCE

at the

Massachusetts Institute of Technology

September, 1979

Signature of Author .....
Department of Materials Science and Engineering
August 10, 1979

Certified by .....
Thesis Supervisor

Accepted by .....
Chairman, Departmental Committee on Graduate Students

ABSTRACT

MASS TRANSFER MODELING OF DRI PARTICLE-SLAG
HEAT TRANSFER IN THE ELECTRIC FURNACE

by

RANDALL STEPHEN WRIGHT

Submitted to the Department of Materials Science and Engineering on August 10, 1979 in partial fulfillment of the requirements for the degree of Master of Science in Metallurgy.

Foaming and turbulent stirring of the slag layer in the electric furnace, produced by the carbon boil, potentially affects the melting rates of DRI particles charged into the slag. Particle-slag heat transfer has been studied with the aid of a low temperature, gas agitated, glycerol-water model in which single and clustered particles of benzoic acid are dissolved; this is a mass-transfer analog for the heat transfer system. By employing Kolmogoroff's theory of locally isotropic turbulence, particle mass transfer rates have been correlated with the variables of fluid kinematic viscosity and power input per unit mass of fluid over a range of Schmidt numbers from 10^3 to 10^6.

The results of the study show that gas entrainment in the liquid phase produces no observable effect on rates of particle mass transfer, and that the mass transfer coefficients for single and grouped particles are equivalent at given values of fluid kinematic viscosity and power input. The experimental findings also indicate that the Sherwood number is not strongly influenced by values of the Schmidt number. The results of the modeling study may thus be employed to infer Nusselt numbers for DRI particles immersed in turbulent slags which have Prantl numbers substantially lower than the Schmidt numbers of the model.

Thesis Supervisor: John F. Elliott
Title: Professor of Metallurgy

TABLE OF CONTENTS

TABLE OF CONTENTS (Cont'd.)

TABLE OF CONTENTS (Cont'd.)

LIST OF FIGURES

LIST OF TABLES

ACKNOWLEDGEMENTS

The author would like to express his appreciation to the members of the Chemical Metallurgy group for their suggestions and useful discussions throughout the course of the present study.

A special note of thanks is extended to Mr. David Cocke for his help in performing many of the experiments.

Professor Kenneth Smith of the Department of Chemical Engineering is gratefully acknowledged for his interest in the author's experiments and his valuable discussions of Kolmogoroff's theory of isotropic turbulence.

The author is especially indebted to Professor John F. Elliott, thesis advisor, for his helpful guidance and encouragement during the author's years at M.I.T.

The National Science Foundation is acknowledged for financial support.

I. INTRODUCTION

Steel production via the electric furnace is now emerging as an economically competitive alternative to the traditional Coke Oven-Blast Furnace-BOF Process. An annual growth rate in total world electric furnace production for the period 1966-1976 of 7.4% (1) clearly underscores the future importance of this technology to the steel industry.

With the tightening of the world scrap market, steel producers have been turning increasingly to the use of pelletized direct reduced iron (DRI) as an alternative feedstock for the electric furnace. This situation is amply demonstrated by a world wide growth in direct reduction capacity since 1958 from approximately 1 Mt to over 20 Mt in 1978, with the greatest increase occurring since 1970 (2).

Despite the fact that the technology for producing steel with direct reduced materials has existed for many years, steel producers are still learning how to take best advantage of the melting chracteristics of DRI. The primary motivation for investigating the melting of D-R materials stems from the need to optimize the melting process and reduce the large energy requirements inherent to electric furnace operations.

Of principal concern to the optimization of melting times during the continuous charging of particles is the identification and analysis of mechanisms which might enhance or inhibit the transfer of heat from molten slags to freely suspended particles of DRI. Based upon the work of Elliott, Nauman, and Sadrnezhaad (3) three mechanisms may be broadly defined which affect the transport of heat in the slag-pellet system (see Fig. I).

1. As particles are fed into the furnace a slag shell solidifies on the surface of individual particles;

2. Because particles are partly composed of FeO and carbon, local outgassing of CO from particles occurs according to the reaction

$$FeO + C + Heat \rightarrow Fe + CO;$$

3. Carbon monoxide gas, formed at the surface of the furnace hearth refractory lining, bubbles through the molten metal and slag layers producing a violent stirring action (henceforth termed carbon boil).

The first two mechanisms have been studied extensively (3, 4, 5). However, the remaining mechanism has received only minor attention by Nauman (4). It is thus the purpose of the present investigation to examine the heat transfer implications of the action of the furnace carbon boil.

Specifically, the bubbling of carbon monoxide through the slag melt creates four conditions which potentially affect heat transfer:

1. large scale turbulence in the slag layer,

2. foaming of the slag,

3. the agglomeration of particles into clumps or islands, and

4. the direct interaction of particles with large bubbles rising through the melt.

The present work seeks to evaluate the significance of the aforementioned carbon boil effects through a modeling of particle slag heat transfer by a mass transfer analogy. In undertaking investigation, use has been made of a low temperature, bubble agitated,glycerol-water bath in which spherical, neutrally buoyant particles of benzoic acid are

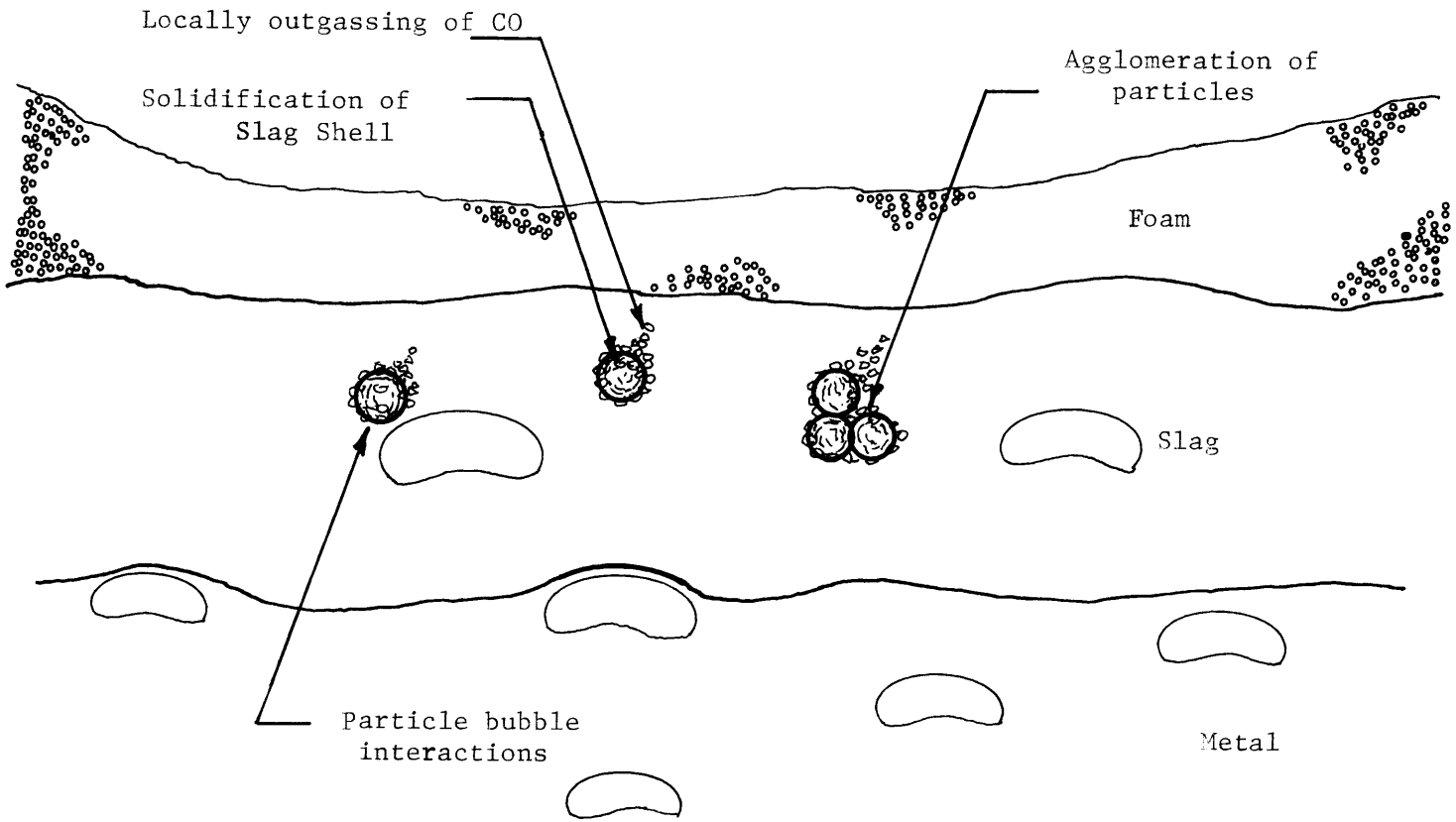

Figure 1 - Mechanisms Affecting Heat Transfer to DRI Particles

dissolved. Dimensional analysis based on Kolmogoroff's theory of locally isotropic turbulence is employed to interpret experimental findings.

The results of the study are presented in the following sequence: recent investigations of turbulent flow in metallurgical systems are first reviewed with an emphasis toward justifying the use of Kolmogoroff's theory of locally isotropic turbulence as a foundation for the present wori; experimental objectives are then elaborated and a rationale is given for basing the experiment on a heat-mass transfer analogy; the apparatus and experimental procedures are next described in detail; experimental results are then presented with an accompanying discussion of data reduction methods and error analysis; finally, results are evaluated in view of Kolmogoroff's theory and the previously mentioned carbon boil effects.

II. PREVIOUS WORK - TURBULENCE STUDIES OF METALLURGICAL SYSTEMS

Preface

In recent years, many investigations of turbulent flow in metallurgical systems have been reported (6 - 11). In order to provide a base from which to evaluate these publications, an outline of the fundamentals of turbulent fluid flow theory is first presented. [A complete treatment of classical turbulence theory is given by Hinze (12).] The following development will also serve to introduce Kolmogoroff's theory of locally isotropic turbulence which is the theoretical foundation of the present work.

A listing of the nomenclature which is used throughout this thesis is given in Appendix H.

II.A. Basic Concepts of Turbulent Flow

The formal analysis of laminar or turbulent flow begins with the consideration of fluid velocities and the Navier-Stokes equations of momentum which embody Newton's Second Law.

Instantaneous fluid velocities are represented at fixed points in the flow as functions of time; this method of describing velocities in time and space coordinates is known as eulerian formulation of motion. In cartesian form, the eulerian velocity vector field is defined:

$$V(r,t) = V(x,y,z,t)$$

$$= iU(x,y,z,t) + jV(x,y,z,t) + kW(x,y,z,t)$$

The Navier-Stokes equations describe the forces acting on a fluid element in a flow field. For the flow of a fluid of constant viscosity under laminar conditions, the equations may be written vectorially as:

$$\underset{\text{I}}{\rho\frac{DV}{Dt}} = \underset{\text{II}}{\rho g} - \underset{\text{III}}{\nabla p} + \underset{\text{IV}}{\mu\nabla^2 V} \qquad \text{(II.1)}$$

The terms of the above equation are interpreted below:

I

(Applied force per unit volume on the fluid element) =

II

(Gravitational body force per unit volume) +

III & IV

(Surface forces: normal and tangential)

The equations can be solved for laminar flows although only a limited number of particular solutions exist.

The Navier-Stokes equations are also valid for turbulent flow, but fluid velocities must be defined in a way which includes the random nature of turbulence. Reynold's (13) proposed that a turbulent quantity Q (e.g., instantaneous velocity, pressure, or temperature) could be defined as the sum of a time averaged or mean value $\bar{Q}$, plus a fluctuating value, q. Thus,

$$Q = \bar{Q} + q \qquad \text{(II.2)}$$

where

$$\bar{Q} = \frac{1}{T}\int_{t_o}^{t_o+T} Q\,dt$$

If the turbulence definitions for velocity and pressure are substituted into Equation (II.1) there results:

$$\rho\frac{D\bar{V}}{Dt} + \rho\frac{\partial}{\partial x_j}\left(\overline{u_i u_j}\right) = \rho g - \nabla\bar{P} + \mu\nabla^2\bar{V} \qquad \text{(II.3)}$$

Comparison of equations (II.1) and (II.3) shows that an additional term, $\rho\partial/\partial xj(\overline{u_i u_j})$, the turbulent inertia tensor, appears in the formulation of the equations for the turbulent case. This term is always significant in any turbulent shear flow and presents an impassed to further analytic treatment because the analytic form of $\overline{u_i u_j}$ is not known à priori. The time averaging procedure, or turbulence definition, introduces nine new variables which can only be defined through a detailed knowledge of the structure of the turbulence. The components of $\overline{u_i u_j}$ are related not only to fluid properties but also to local flow conditions of velocity, geometry, and upstream history. No further conservation laws can be applied to aid in a solution. However, sets of auxiliary equations have been proposed to remedy this dilemma; such sets of additional equations constitute what are known as turbulence models.

II.B. Turbulence Models and Metallurgical Applications

The turbulent inertia terms of Equation (II.3) can be rewritten as if they were stresses and incorporated with the tangential stress terms:

$$\frac{D\bar{V}}{Dt} = \rho g - \nabla\bar{P} + \nabla.\tau_{ij} \qquad \text{(II.4)}$$

where

$$\tau_{ij} = \underbrace{\mu\left(\frac{\partial u_i}{\partial xj} + \frac{\partial u_j}{\partial xi}\right)}_{\text{LAMINAR}} - \underbrace{\rho(\overline{u_i u_j})}_{\text{TURBULENT}} \qquad \text{(II.5)}$$

The terms represented by $\rho(\overline{u_i u_j})$ are known as the "Reynold's Stress" components of the total stress tensor.

Turbulence models allow a quantitative prediction of fluid velocity fields, and system kinetic energy distributions, through equations which model the "Reynold's Stress" components of the turbulent Navier-Stokes

equations. The precise details of the models are not a part of the present work; it will only be noted here that the models which have been proposed to date are restricted to two-dimensional flows. (A complete elaboration of turbulence modeling is given by Launder and Spalding (14, 15).

Previous studies of turbulence in metallurgical systems where axi-symmetric recirculating flows are present have concentrated heavily on the use of turbulence models. For example, Guthrie and Salcudean (6) have studied the fluid flow encountered during tapping operations from a basic oxygen furnace by employing the modeling techniques of the Los Alamos (16) and Imperial College groups (17). Tarapore and Evans (7) calculated fluid velocity profiles in induction melting furnaces through the simultaneous solution of the Maxwell and Navier-Stokes equations and utilization of Spalding's K-W model (15). In a similar direction, Dilawari et al. (8, 9) have modeled heat transfer and flow phenomena for the ESR and ESW processes, while Szekely and Chang (10) have extensively studied electromagnetically driven flows in liquid metals.

Despite the variety of these investigations, the only study which is even remotely similar to the present work is that of Szekely, Wang, and Kiser (11) for which Spalding's two equation K-W model was applied to a water simulation of an argon stirred ladle. The principal difference between the turbulent electric furnace slag system and the case of an argon stirred ladle is that in the Szekely model agitation was provided by a single bubble column; thus, symmetry about a vertical axis was preserved. In contrast, a boiling system involves a three-dimensional flow created by many bubble columns.

Additionally, complications arise for the boiling system in prescribing the boundary conditions of the modeling equations for the flexible slag-metal interface and in relating the calculated fluid velocity vector field to the boundary layers of particles carried in the flow.

The analysis of turbulent slag-particle heat transfer must therefore be founded in an approach other than the current trend of turbulence modeling. Fortunately, Kolmogoroff's theory of locally isotropic turbulence and the Brian-Hales correlation which is based upon this theory provide a suitable alternative theoretical framework.

II.C. Kolmogoroff's Theory of Locally Isotropic Turbulence

Turbulent velocities present two types of information which characterize a flow field. Direction is, of course, specified, but kinetic energy is also implied by the fluctuating components.

Fluid eddies which make up the flow contribute to fluctuations in the velocity vector field. Eddies are identified by their frequency $n(sec^{-1})$, or by a wavenumber k; the physical size or length scale of an eddy is inversely proportional to its wavenumber.

Eddies are related to velocity fluctuations through an energy spectrum function. If a flow field is quasi-steady so that it is statistically homogeneous with respect to time, then there exists a constant average value of the system turbulence kinetic energy u^2, which consists of the sum of the contributions of all eddy frequencies n. If E(n) dn is the energy contribution of eddies of frequency n + dn to the total kinetic energy $\overline{u^2}$, an energy distribution function may be written:

$$\int_0^\infty E(n)\, dn = \overline{u^2} \tag{II.6}$$

or, in terms of the wavenumber k,

$$\int_0^\infty E(k)dk = \overline{u^2} \tag{II.7}$$

Figure II shows the distribution of turbulence kinetic energy over the range of wavenumbers from zero to infinity. The area under the curve between any two wavenumbers is equal to the energy content of eddies within that wavenumber range.

Kolmogoroff (18) proposed that high levels of turbulence result in the inertial transfer of energy from low to high wavenumber eddies. Ultimately, all energy is dissipated viscously in the smallest scale eddies. Because the transfer of energy occurs in many directions, the directional information from the primary (i.e., low wavenumber) eddies is successively lost as the transfer process proceeds. Hence, the only information which is finally conveyed from primary to dissipation eddies is an energy content.

Through Kolmogoroff's theory the eddy size distribution of Figure II may be divided into three groups.

The largest eddies of the distribution comprise the first group. These low wavenumber eddies may contain as much as twenty percent of the total system kinetic energy; however, the amount of energy they contain is dependent upon how the turbulence is generated. For example, an impeller stirred system may produce an energy spectrum in the low wave-

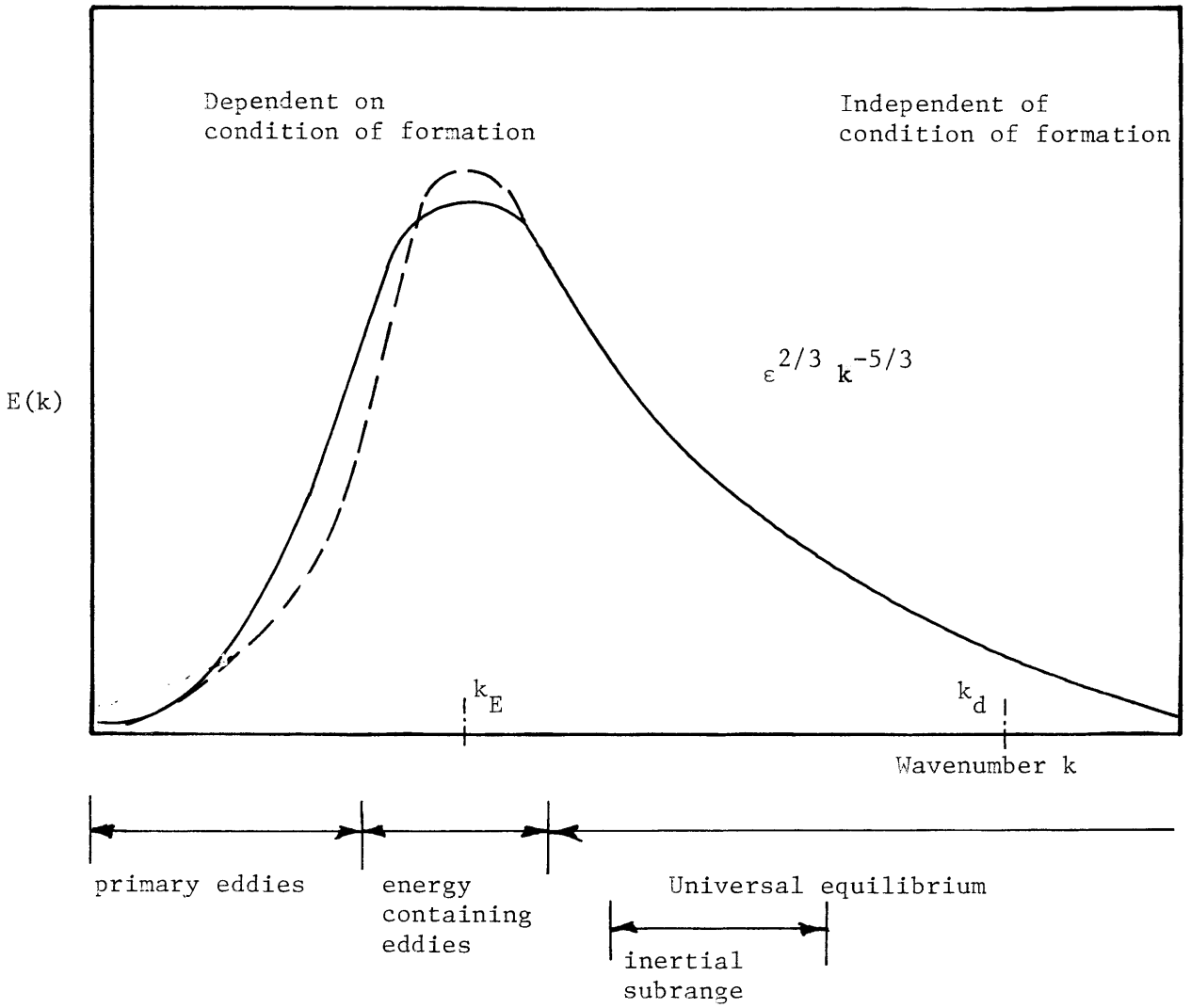

Figure II - Energy Spectrum

number range which differs from, say, a bubble agitated system. This is illustrated by the dashed and solid curves of Figure II which depict the low wavenumber spectrum for a system agitated by two different means.

Intermediate size eddies with wavenumbers ranging around k_E make up the second group. They contain most, and dissipate only a negligible portion, of the total system kinetic energy.

Eddies with wavenumbers in the range of $k_d >>> k_E$ constitute the last group. All turbulent kinetic energy is dissipated in this range of the spectrum through viscosity into heat. The high wavenumber eddies are independent of the conditions of their formation (i.e., this portion of the spectrum remains unchanged regardless of the method of agitation) and are said to comprise the universal equilibrium range of wavenumbers. These eddies are directionally independent of the main flow; in terms of the fluctuating velocity components discussed earlier, $\overline{u^2} = \overline{v^2} = \overline{w^2}$ for high wavenumber eddies only. The small eddies thus represent <u>locally</u> isotropic turbulence.

Kolmogoroff postulated that within the universal equilibrium range the energy spectrum would be a function only of the energy dissipation per unit mass (ε) and the tendency of the fluid to dissipate energy through viscosity (ν). He further stated that for high levels of turbulence the energy spectrum in the region $k_E << k << k_d$ would be independent of ν and solely dependent on ε; eddies within this range of wavenumbers form the inertial subrange of the energy spectrum.

Through purely dimensional reasoning Kolmogoroff deduced the spectrum law for the inertial subrange (see Figure II):

$$E(k) = A\varepsilon^{2/3} k^{-5/3} \qquad \text{(II.8)}$$

The above equation, which is known as Kolmogoroff's Spectrum Law, has been verified through the investigations of Grant et al. (19) and Von Kármán (20).

Although Kolmogoroff's theory deals strictly with fluid turbulence it also provides insight into the mechanics of particle heat and mass transfer. A particle which is carried in a turbulent flow may be considered to experience two extreme environments:

1. A conveying environment in which the particle is entrained in an eddy larger than the particle itself and is transported through the fluid;

2. A convection environment in which eddies, the same size as the particle or smaller, move over the particle surface and produce a convective transfer of heat or mass.

If the particle is equal in size to eddies in the universal equilibrium range of the energy spectrum it may be expected that the rate of convective transfer will depend upon the variables ν and ε. Brian, Hales, and Sherwood (21) made this assumption in their development of a dimensionless correlation which allows the prediction of heat and mass transfer rates for particles suspended in turbulent flows.

II.D. Brian-Hales Correlation

The analysis of heat and mass transfer for particles suspended in a turbulent flow should incorporate some notion of a relative velocity between a particle and its surrounding fluid. Expressions for the relative velocity between two points in a flow can be derived through

dimensional consideration of ε and ν.

Following the development of Shinnar and Church (22) let r_1 and r_2 represent two points in the flow. r is equal to the radius vector $r_1 r_2$ and is assumed to be small in comparison to the length scale of the large primary eddies, L. The relative velocity $\overline{u^2(r)}$ between the two points may then be defined:

$$\overline{u^2(r)} = \overline{[u(r_1) - u(r_2)]^2} \tag{II.9}$$

From the foregoing discussion of the energy spectrum function it can be stated that the primary eddies (which are much larger than r) will contribute negligibly to $u^2(r)$; if r is much smaller than the length η of dissipation eddies which have wavenumbers ranging about k_d, then the relative velocity should depend primarily upon ε and ν. For $r << \eta$

$$u^2(r) = C_1 \frac{\varepsilon}{\nu} r^2 \tag{II.10}$$

If r is roughly equal in size to eddies in the inertial subrange of the spectrum, then $\overline{u^2(r)}$ should be independent of viscosity and a function only of ε in agreement with Kolmogoroff's Spectrum Law. Thus, for $L >> r >> \eta$

$$u^2(r) = C_2 \varepsilon^{2/3} r^{2/3} \tag{II.11}$$

This expression has been experimentally verified by Kuboi, Komasawa, and Otake (23).

The values of $\overline{u^2(r)}$ for expressions (II.10) and (II.11) are independent of the direction of the radius vector r, in accord with the assumption of local isotropy.

The Brian-Hales correlation is built upon the relative velocity expressions given above. The derivation of the correlation begins with the representation of relative fluid velocities in dimensionless form and the assumption that this velocity representation is a function of a dimensionless group incorporating ν and ε. Thus,

$$\frac{\sqrt{\overline{u^2(r)}}\, r}{\nu} = f\left(\frac{\varepsilon r^4}{\nu^3}\right) \qquad \text{(II.12)}$$

The group on the left of Equation (II.12) is the Reynold's number of the fine scale turbulence. If eddies approximately equal in size to the particle diameter d are considered to be primarily responsible for convection, then d may be substituted for r in the above equation to yield an expression for the fluid velocity over the particle surface:

$$\frac{\sqrt{\overline{u^2(r)}}\, d}{\nu} = f\left(\frac{\varepsilon d^4}{\nu^3}\right) \qquad \text{(II.13)}$$

Dimensionless correlations for particle heat and mass transfer have long been based upon boundary layer theory (24, 25). Schlicting (26) has shown that in the case of forced convection the dimensionless convective transfer coefficient (i.e., Nusselt or Sherwood numbers) is a function of only two dimensionless groups:

$$Nu = f(Pr, Re) \qquad \text{Heat transfer} \qquad \text{(II.14)}$$

and

$$Sh = f(Sc, Re) \qquad \text{Mass transfer} \qquad \text{(II.15)}$$

where,

$Nu = \frac{hx}{k}$ Nusselt number

$Pr = \frac{\nu}{\alpha}$ Prandtl number

$Sh = \frac{h'x}{D}$ Sherwood number

$Sc = \frac{\nu}{D}$ Schmidt number

$Re = \frac{ux}{\nu}$ Reynold's number

Consequently, any correlation which is based upon the idea of a relative velocity between turbulent eddies and a particle's surface will be of the form shown in Equations (II.14) and (II.15); a substitution of $(\frac{\varepsilon d^4}{\nu^3})$ for Re can therefore be made:

$$Nu = f(Pr, \frac{\varepsilon d^4}{\nu^3}) \tag{II.16}$$

and

$$Sh = f(Sc, \frac{\varepsilon d^4}{\nu^3}) \tag{II.17}$$

The parameter $(\frac{\varepsilon d^4}{\nu^3})$ is called the Kolmogoroff number and is designed Ko.

If a simple power law expression, similar in form to the correlations for particle dissolution of Frossling (24) or Ranz and Marshall (25), is used to represent Equations (II.16) and (II.17) there results:

$$Nu = APr^{x_1} Ko^{x_2} \tag{II.18}$$

and

$$Sh = ASc^{x_1} Ko^{x_2} \tag{II.19}$$

The exponent x_1 of Pr and Sc was set equal to 1/3 by Brian and coworkers (21) based on boundary layer theory and the relative velocity argument given previously. (If, for example, the assumption had been made that $r \ll d$ in Equation (II.12), then small eddies would have been considered primarily responsible for heat or mass transfer through a

mechanism of surface renewal in which small fluid eddies attach to a particle's surface, transfer heat or mass through conduction or diffusion, and then move away into the bulk fluid; under this model the exponent x_1 would be taken to be equal to 1/2. Further discussion of the choice of the power dependency of Pr or Sc is given by Schlicting (26), and Danckwerts (27, 28).

The form of the correlation was verified, and the power dependency of Ko determined to be 1/6, through a calorimetry experiment conducted by Hales (29) in which ice particles, 2.4 mm in diameter, were melted in a 2.3 liter impeller stirred reactor filled with water (Pr = 13.7). Additional mass transfer experiments were conducted by measuring the rate of solution of particles of pivalic acid ($C_5H_{10}O_2$) ranging in size from 1.5 to 3.0 mm in diameter (Sc = 3200). Power input per unit mass of fluid (ε) was determined by measuring the torque applied to the vessel during agitation.

By experiment the correlation takes final form as:

$$\frac{Sh}{Sc^{1/3}} = 1.17\ Ko^{0.17} \quad \text{Brian-Hales correlation (II.20)}$$

Figure III shows Hales' (29) results accompanied by the ion exchange resin data of Harriott (30) for values of Sc ranging from 518 to 107,500. The deviation between the results for different values of Sc or Pr indicates that the 1/3 exponent of the Schmidt and Prantl numbers is not adequate in correlating the data. Therefore, the assumption of a slip velocity transfer mechanism may not be completely correct. Brian et al. (21) have only noted the deviation and have not given any detailed explanations for the trend in the results.

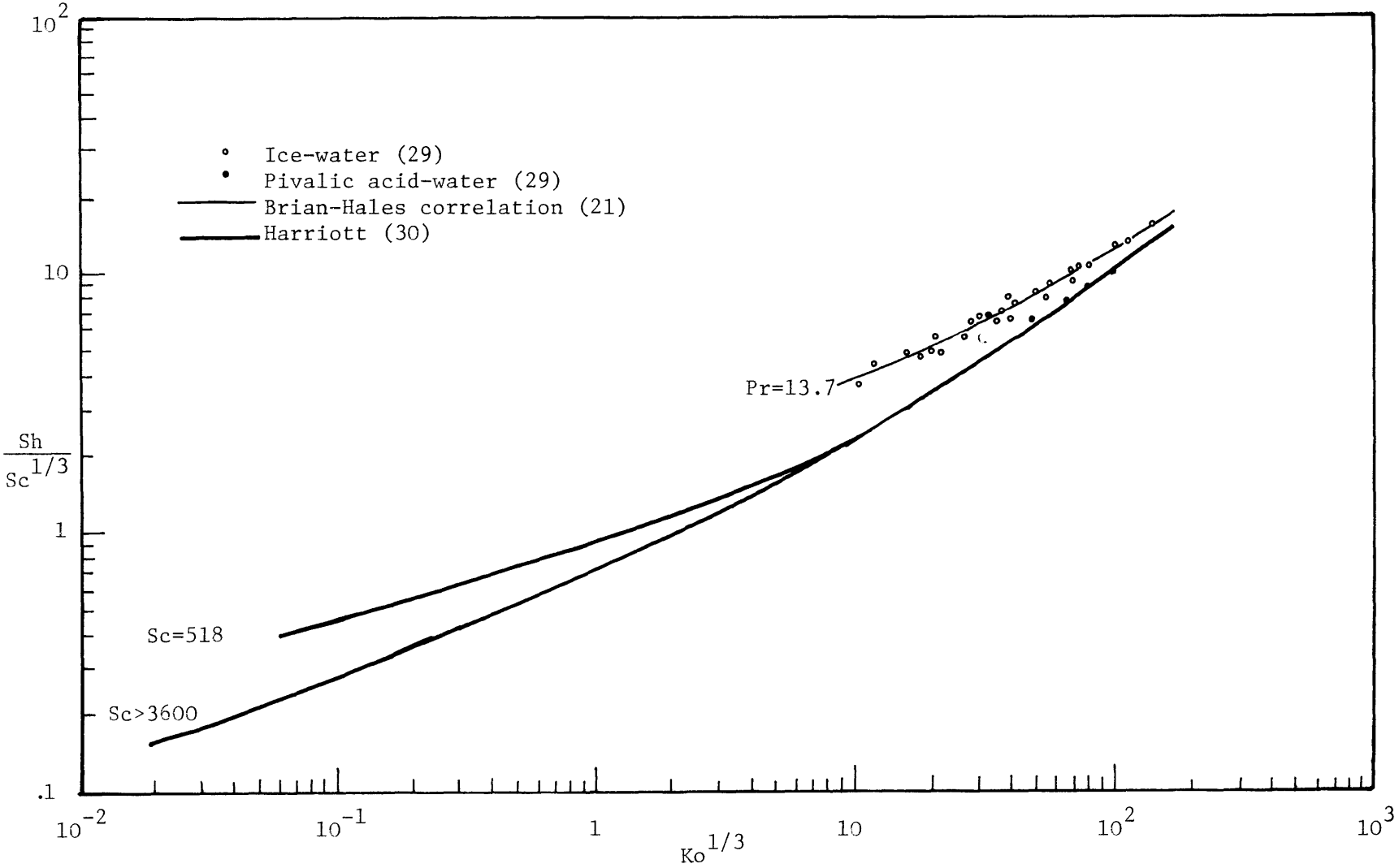

Figure III - Brian-Hales Correlation

The usefulness of any correlation for agitated reactors depends upon the accuracy with which results of small scale experiments can be extrapolated to large industrial systems. Wadia (31) focussed on this issue in his extensive investigation of the Brian-Hales correlation for large systems. Experiments were conducted for a wide variety of vessels (ranginf from 14.1 cm to 183 cm in diameter) and impeller geometries. Particles of pivalic acid ($C_5H_{10}O_2$), iso-valeric amide ($C_4H_{11}ON$), brassidic acid ($C_{22}H_{42}O_2$), and benzoic acid ($C_7H_6O_2$) ranging in size from 0.25 to 2.25 cm in diameter were dissolved in water and solutions of glycerol and water. Schmidt numbers varied from 10^3 to 10^6.

One of the most important outcomes of the study was the identification of three mass transfer regimes which were found to depend on particle size and the wavenumber denoting the onset of universal equilibrium. In the present work only the large particle regime is of interest; Wadia's (31) results for this regime are shown in Figure IV.

A systematic deviation is evident between the results for large particles and the correlation line for small particles with diameters similar in size to the length scales of isotropic eddies. This deviation has been attributed by Wadia (31) to be due to the eddies which contribute to mass transfer in the large particle regime; the wavenumbers of these eddies fall outside of the universal equilibrium range ($k<k_E$) so that effective slip velocities are partly dependent upon vessel diameter and impeller geometry.

It may be inferred from Figure IV that although the vessel size and the method of agitation may influence values of the Nusselt or Sherwood

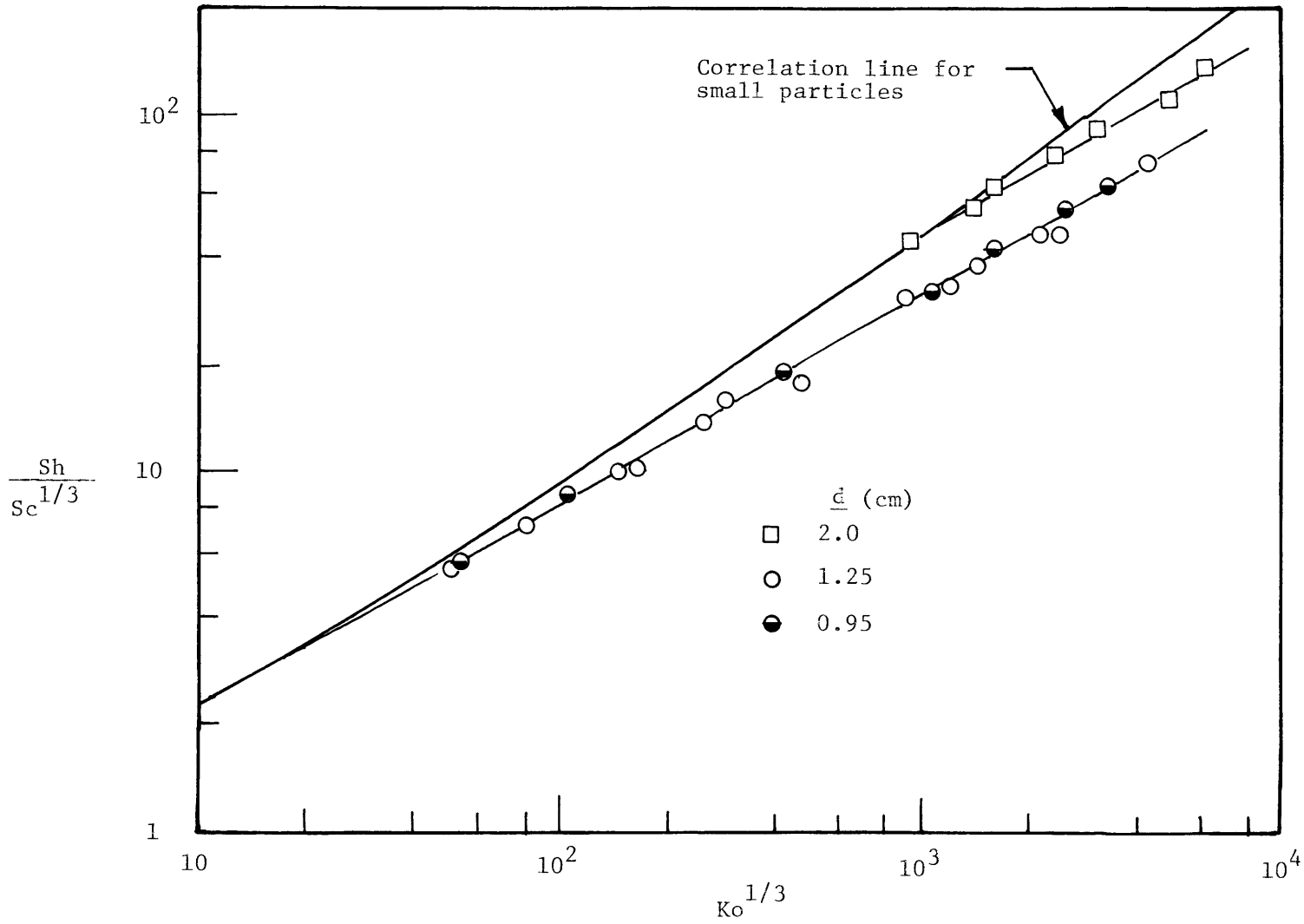

Figure IV - Results of the Study of Wadia (31) for Large Particle Regime

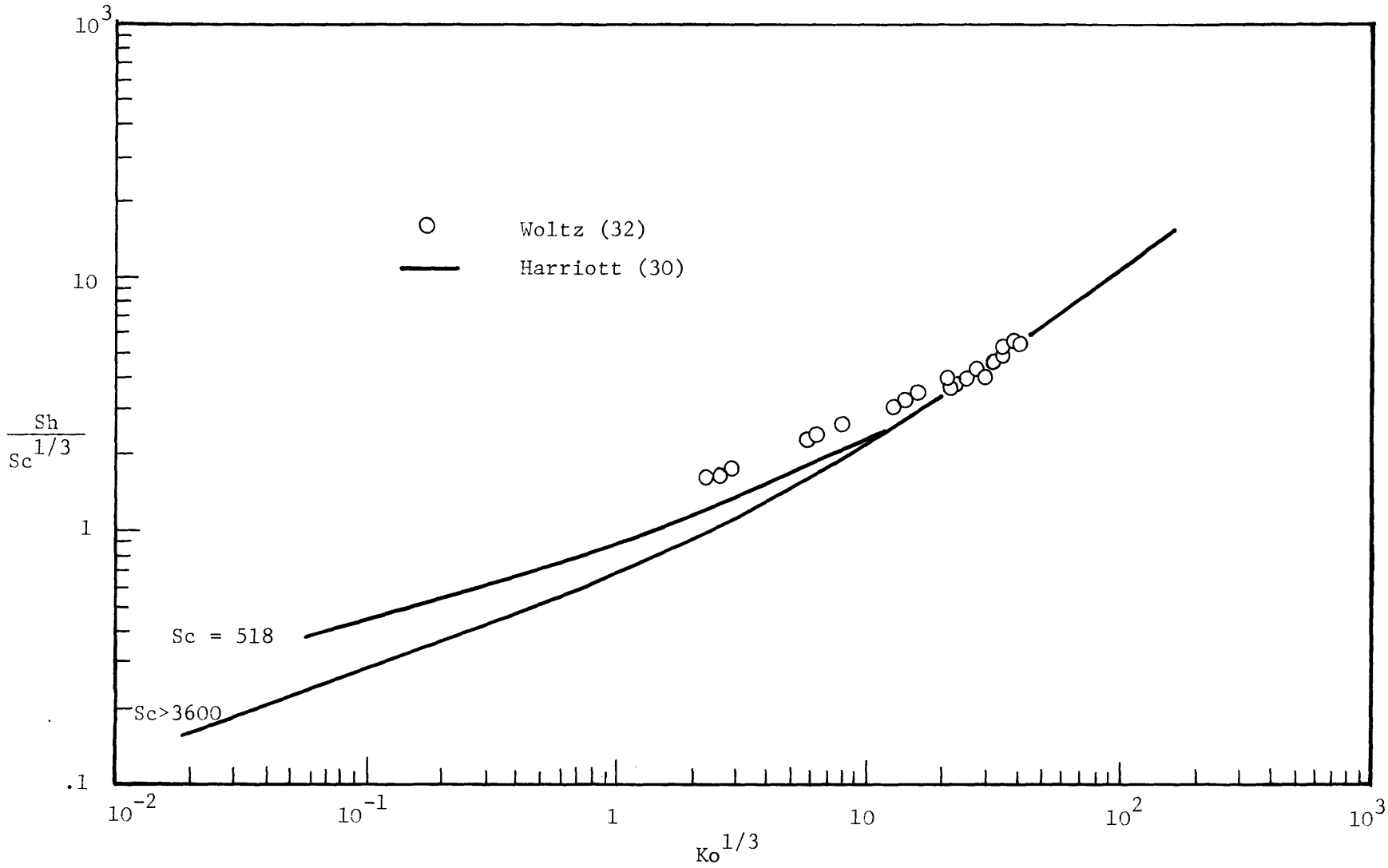

Figure V - Results of the Study of Woltz (32) for Gas Agitation

numbers for large particles, results can still be effectively correlated on the basis of the variables ε and ν in the large particle regime.

Woltz (32) has examined the correlation for a small, 1 liter, bubble agitated water system in which spherical Dowex resin beads (40 to 850 microns in diameter) were employed to determine convective mass transfer coefficients. Power input was determined through a thermodynamic consideration of the action of rising gas bubbles. The results are shown in Figure V together with the data of Harriott (30) which is included for comparison.

The results confirm the assumption that the amount of power input, and not the source of agitation, is a primary factor in correlating the data.

II.E. Significance of the Brian-Hales Correlation to Metallurgical Systems

Nauman (4) has included the correlation in a computer simulation of electric furnace charging and melting operations. He also applied the correlation in a laboratory experiment where the solidification of slag on the surfaces of 3 cm diameter nickel spheres was produced in a small 15.25 cm diameter crucible; agitation was created by bubbling nitrogen through the melt. However, no large scale studies have been undertaken to test the validity of the Brian-Hales correlation for the DRI particle-slag system.

From a review of the foregoing studies it is evident that Brian-Hales correlation provides a potentially useful way of determining Nusselt numbers for DRI particles suspended in turbulent electric furnace slags. This is particularly true in view of the insensitivity of the correlation to variations in agitation method, vessel size, and particle diameter.

III. EXPERIMENTAL DESIGN AND OBJECTIVES

Preface

The primary objective of the present work is to determine if the Brian-Hales correlation can be employed to predict Nusselt numbers for DRI particles immersed in turbulent, gas agitated, electric furnace slags. This objective has been pursued through an experimental investigation; because of the difficulties involved in handling large quantities of slag, particle-slag heat transfer has been modeled through a low temperature, mass transfer experiment. As a result, the objectives of the study also include a test of the validity of the heat-mass transfer analogy.

In what follows, the experimental design criteria are explained and a rationale is given for the use of the mass transfer model. The limitations of the model are then discussed. Finally, the experimental objectives are presented together with a plan of work for the study.

III.A. Design

III.A.1. Modeling Parameters and Furnace Conditions

Table I lists the variables which are important to the design of the experimental model. The design variables include particle diameters and densities, slag properties, and dimensions of the slag layer.

The ratios of particle density (ρ_p) to slag density (ρ_s) calculated from the values of Table I range from 0.56 to 2.0. Brian and co-workers (21) have shown that for neutrally buoyant particles the correlation

$$\frac{Nu}{Sc^{1/3}} = 1.17\ Ko^{1/6} \qquad (II.20)$$

is independent of gravitational effects and differences in phase density.

Table I - Electric Furnace Modeling Parameters and Variables (5, 41)

DRI Particles	
Diameter, cm	1.2
Density, g/cm^3	2 - 6
Slag	
Density, g/cm^3	3 - 3.6
Kinematic Viscosity, cm^2/sec	0.56 - 1.72
Thermal diffusivity, cm^2/sec	0.0040 - 0.0052
Prandtl number	108 - 431
Temperature, °C	1600
Furnace Conditions	
(200 ton furnace)	
Furnace diameter, cm	724
Slag depth, cm	30
CO evolution rate, $\frac{mol}{sec}$	4.20 - 8.40

Particles that are not neutrally buoyant would require a relation of the form

$$Nu = f(Pr, Ko, \frac{gd^3(\rho_p - \rho_s)}{\nu^3 \rho_s}, \frac{\rho_p}{\rho_s}) \qquad \text{(III.1)}$$

in order to correlate experimental data. The gravity group $gd^3(\rho_p - \rho_s)/\nu^3\rho_s$ includes a contribution to the slip velocity produced by particles falling through the flow at their terminal velocities; the density ratio (ρ_p/ρ_s) represents an additional relative velocity which exists as the result of a difference in inertia between the two phases (21). To simplify the interpretation of the experimental findings of the present study it is assumed that DRI particles have densities which are equal to those of electric furnace slags [i.e., $(\rho_p/\rho_s) = 1$].

The particle diameter is significant because the Brian-Hales correlation is based on the assumption that the eddies which are principally responsible for convective transfer are equal in size to particles in the flow. As noted earlier, the wavenumbers of convective transfer eddies in the large particle regime may lie outside of the universal equilibrium range of the energy spectrum; the convective transfer coefficients for large particles may be influenced by the method of agitation and the dimensions of the system. There is no rule or method available to determine if a particle borders on the large particle regime. A limit of the large particle regime diameter cannot be inferred from Figure IV because Wadia's (31) data is for an impeller stirred system; gas agitation may affect experimental results to a greater or lesser degree than impeller agitation. To determine if gas agitation and system boundaries

affect rates of heat transfer, model particles with diameters approaching those of direct reduced materials must be used in the experiment.

The significant slag properties include the kinematic viscosity and the Prandtl number.

Inspection of the Kolmogoroff number ($\varepsilon d^4/\nu^3$) reveals that the kinematic viscosity strongly affects the value of Ko. Simple calculations of electric furnace Kolmogoroff numbers for the CO evolution rates given in Table I, a slag kinematic viscosity of 57 c.s., and a particle diameter of 1.2 cm, show that Ko ranges only from about 30 to 45 (see Appendix A for details).

Since model particle diameters must be close to 1.2 cm, the only way that the Brian-Hales correlation can be tested in the range of electric furnace Kolmogoroff numbers is through a very close matching of the viscosity of the model liquid to that of the slag.

The Prandtl numbers of the model liquid and the slag should be equivalent so that similarity is achieved between the boundary layers of model particles and those of DRI pellets.

Finally, complete similarity between the model and the DRI particle-slag system should include a geometric scaling of the boundaries of the model with those of the slag pool and a modeling of the flexible slag-metal interface. Geometric scaling is only important because non-isotropic eddies may influence the transfer of heat from the liquid slag to DRI particles. If the flow pattern in the slag pool is duplicated in the model the results of the experimental study may be more readily extended to the industrial system.

III.A.2. Rationale for the Heat-Mass Transfer Analogy

As noted earlier, model particles must be approximately equal in size to actual pellets of DRI. This requirement imposes the major restriction that experiments be conducted with a large vessel. Ideally, the experimental vessel should have dimensions equal to those given in Table I for the electric furnace; a full scale experiment however is not practical due to space limitations. In the present work no attempt has been made to either geometrically scale the model system with the slag layer or to model the flexible slag-metal interface. Only a general geometric similarity has been attempted by the use of a cylindrical tank and a liquid depth of 30 cm corresponding to an average thickness of the slag layer. The implications of this non-geometric scaling are discussed in Chapter VI.

An appropriate tank size can be inferred from previous investigations of the Brian-Hales correlation; if the ratio of tank to particle diameter of the study of Brian and co-workers (21) is used as a rough size estimate it may be seen that this ratio should equal about fifty. A reasonable experimental study requires at least a 60 cm diameter vessel for 12 mm particles; for a liquid depth of 30 cm, the experimental system would have a volume of about 85 liters.

As a result of the equivalency of heat and mass transfer illustrated by the Brian-Hales correlation in Figure III the choice of a heat or mass transfer method rests largely upon the difficulties involved in the execution of large scale experiments by each alternative.

Of the two methods, heat transfer experiments represent the least

desirable alternative. This is a result of the following:

1. If a calorimetry experiment similar to the type that Hales (29) conducted is attempted on a larger scale, huge quantities of pellets are required to effect a small change in the fluid temperature due to the large heat capacity of the bath;

2. A small temperature change is difficult to measure and necessarily demands precise equipment to develop accurate data;

3. To maintain accuracy, the outer boundaries of the system must be heavily insulated, and all heat losses must be accounted for.

In contrast, mass transfer experiments involve simple measurements and require only modest equipment, yet offer the same type of data provided by heat transfer experiments.

Following the work of Wadia (31) the decision was made to employ a glycerol-water system, for which viscosity could be easily varied, and spherical particles of benzoic acid. This alternative was especially attractive inasmuch as the appropriate references for solution viscosity and solute diffusivities were readily available.

The diffusivities of benzoic acid in water or solutions of glycerol and water are on the order of 10^{-7} cm^2/sec and presented an additional advantage: the use of an acid with a low diffusion coefficient minimized the effect of particle shrinkage on the Sherwood number. Thus, experimental results were rendered on a more comparable level to the real system where DRI particles are assumed to be spheres of fixed diameter.

Preliminary laboratory investigations of the foaming ability of glycerol-water solutions with viscosities ranging from 2.5 to 42 c.s.

demonstrated that these solutions would form gas emulsions (i.e., entrain <10% gas by volume as defined by Levich (33). Thus, the effects of slag foaming could be studied in a simplified way. (See Chapter VI for further details.)

III.A.3. Limitations of the Analogy

The greatest limitation created by utilization of a glycerol-water/benzoic acid system arises in terms of matching the model viscosity and Schmidt number to the slag viscosity and Prandtl number. Slags used by Nauman (4) and Sadrnezhaad (5) had viscosities ranging from 56 to 172 c.s. and corresponding values of Pr from about 100 to 430. The slag viscosity can easily be matched with a solution of glycerol and water. However, the Schmidt number for a glycerol-water/benzoic acid system with a viscosity of 57 c.s. will equal about 10^6. This situation cannot be remedied with a small change (i.e., decrease) in viscosity since the Schmidt number changes only moderately with viscosity (see Figure VI). Furthermore, benzoic acid in water (ν = 1cs) will still evidence a value of Sc of about 1000 at 20°C.

Observation of the data shown in Figure III shows that values of $(Sh/Sc^{1/3})$ are only influenced by Schmidt numbers less than 3600. At a Kolmogoroff number of one, the difference in the value of $(Sh/Sc^{1/3})$ for Schmidt numbers of 518 and 3600 is 22%. For values of the Kolmogoroff number greater than 10, the Schmidt number has no apparent effect on the value of the ordinate group. In light of these data it would seem that a very high Schmidt number may not invalidate model results in the low Kolmogoroff number range for application to the electric furnace slag

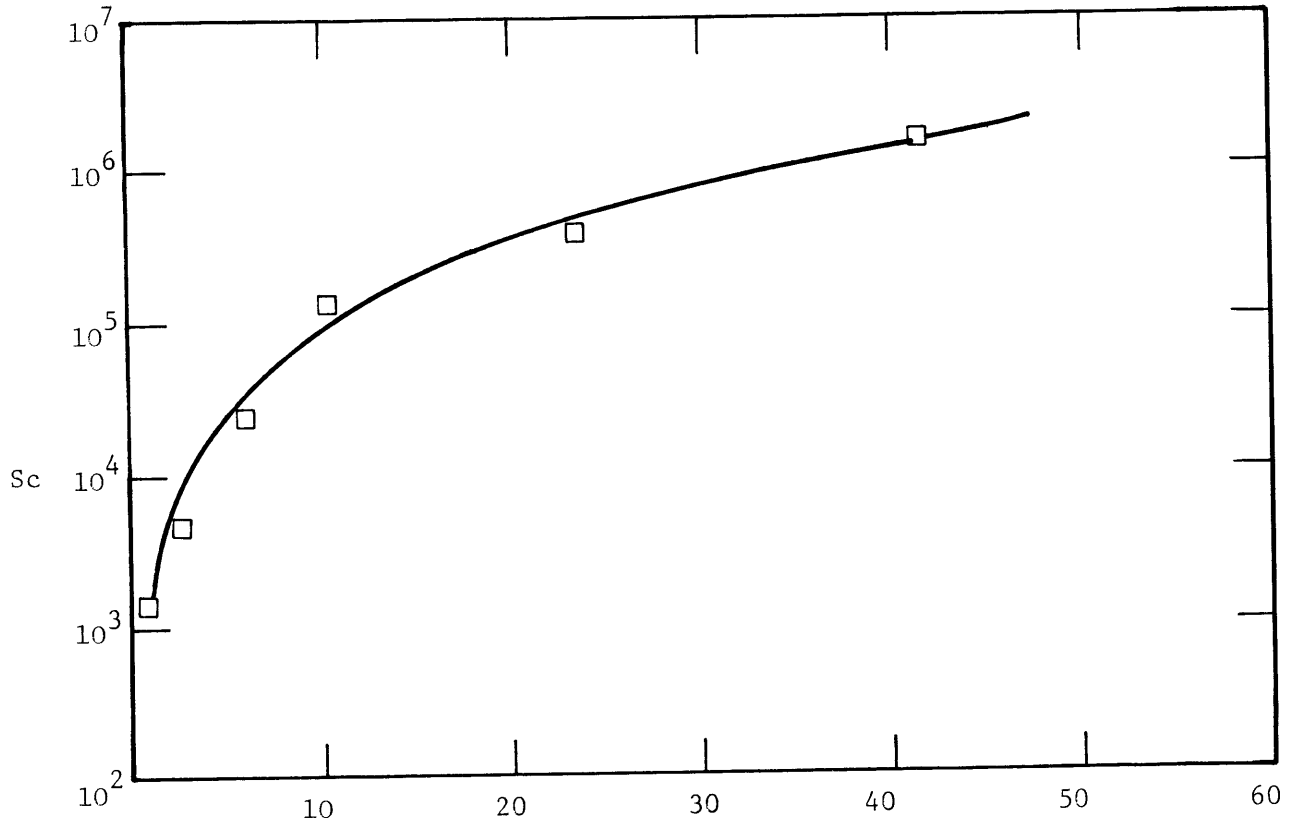

Figure VI - Sc vs. ν for Glycerol-Water Solutions

system.

Despite the convenience of the mass transfer method, the overall experimental objectives must include investigation of the influence of Schmidt number on the Sherwood number in order to establish the validity of the heat-mass transfer analogy.

III.B. Experimental Objectives

Four experimental objectives are part of the overall goal of testing the Brian-Hales correlation for the DRI particle-slag system:

1. to test the correlation for the range in $N_{ko}^{1/3}$ of 20-35 corresponding to actual furnace conditions,

2. to establish the effect of the Schmidt number of the Sherwood number,

3. to assess the importance of entrained gas on the transport process, and

4. to determine the significance of particle agglomeration on the convective transport coefficients of individual particles.

The first objective was undertaken by matching the Kolmogoroff number of the model to that of an electric furnace system. The matching was achieved by approximating the viscosity of a slag with a glycerol water solution (ν_{model} = 42 cs).

To check the effect of Sc, a broad spectrum of experiments were run for $Ko^{1/3}$ ranging from 19 to over 1000, where Sc varied from 1000 to 10^6. Thus, any effect can be observed as a general trend when the data are plotted according to the correlation.

The third objective was pursued by comparing experimental results for the glycerol-water solutions, which evidence gas entrainment, with those of water solutions where entrainment was absent.

The last objective was accomplished by studying the dissolution of paired and tetrahedrally arranged particles over the entire viscosity range. These results will be compared with those for single particles.

The entire plan is summarized in Table II.

Table II - Work Plan

Experimental group	Solution composition (wt. per cent glycerol)	$\nu_{c.s.}$	Sc	$Ko^{1/3}$
1	79	41.6	1.532×10^6	20-30
2	72	23.7	5.516×10^5	30-54
3	64.2	10.5	1.088×10^5	84-95
4	55	6.0	3.716×10^4	134-187
5	34	2.5	6.768×10^3	338-500
6	(pure water)	1.0	1.215×10^3	800-1270

NOTE: 1. Group 6 - No entrained gas

2. All groups include tests for single, paired, and tetrahedrally arranged particles.

IV. APPARATUS AND PROCEDURE

IV.A. Apparatus

The apparatus used in the present set of experiments is shown in Figure VII. The system includes the following components:

1. A large polyethylene tank, 55.9 cm in diameter, fitted with a plexiglass window,
2. a sparger (perforated plate),
3. a rotary vane air compressor, and
4. an air flow and metering system.

The polyethylene tank was equipped with a plexiglass window (28 cm x 38 cm) covering a 90° sector of the circumference of the tank which allowed viewing of general flow patterns, and interactions of particles with bubble columns and small entrained gas bubbles. The window was fabricated from a 3.2 mm thick plexiglass sheet which was first heated in an air furnace to 125°C for 20 minutes and then shaped to fit the inside diameter of the tank. The sheet, when cool, conformed to the tank radius. The curved sheet was installed inside the tank together with a gasket made of 1.6 mm latex rubber. Strips of aluminum were fitted on the outside of the tank to provide a rigid frame for the window. The entire assembly was held together with 32 4.76 mm diameter aluminum bolts.

A sparger 45.7 cm in diameter was constructed from two 3.2 mm and one 9.5 mm sheets of aluminum. Gaskets were cut from a 1.6 mm latex rubber sheet. A weight made of 6.4 mm steel plate was attached to the under-side of the sparger to hold the unit in place during its operation.

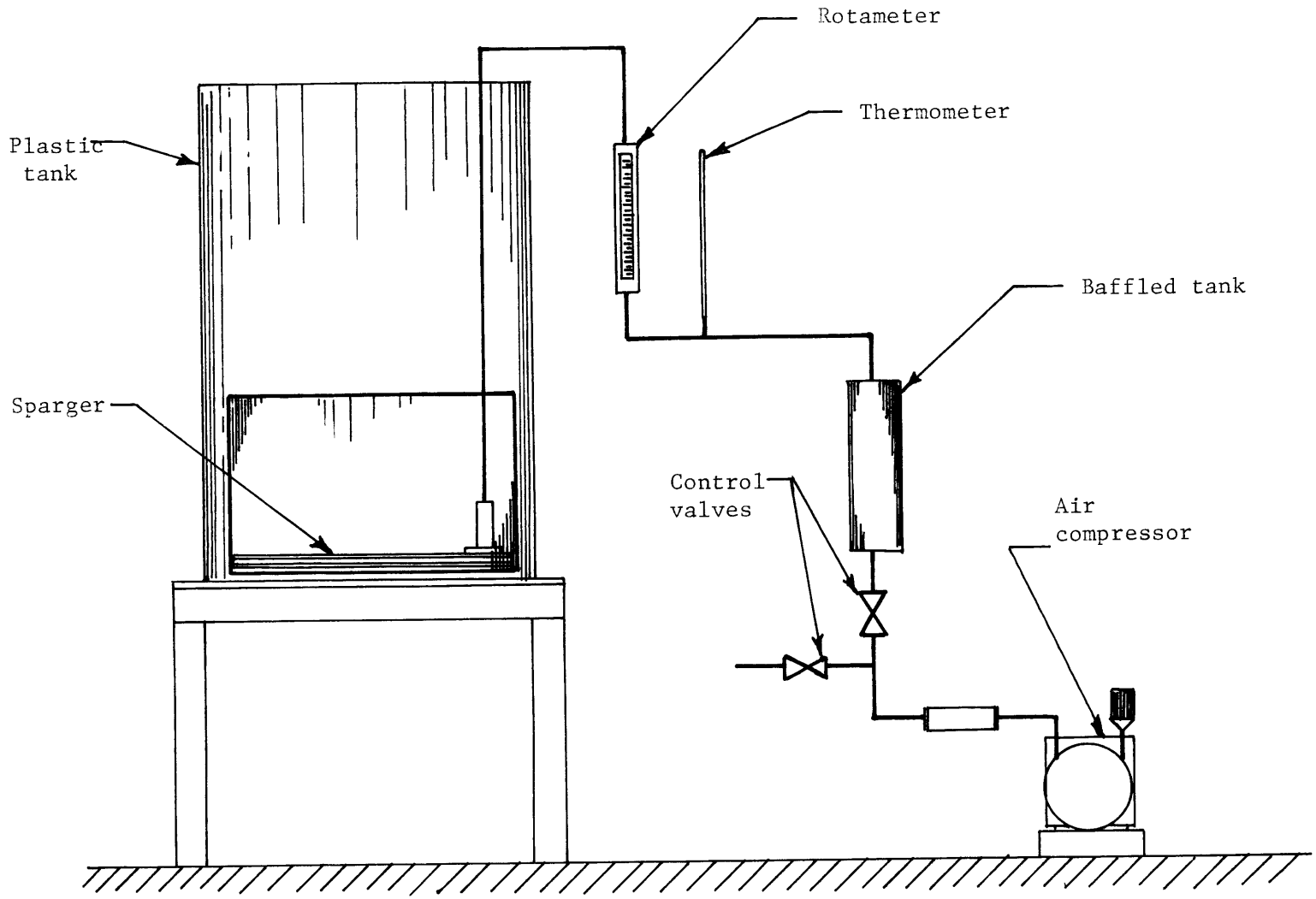

Figure VII - Experimental Apparatus

Details of the sparger's construction are given in Figure VIII.

A small rotary vane air compressor (#1022-P102-G272X manufactured by Gast Inc., Benton Harbor, Michigan) was employed to supply the necessary air flow to the sparger (maximum 280 1/min @ 0 atm gauge pressure). This compressor was chosen because the rotor vanes were made of carbon which eliminated any possibility of oil being present in the incoming air. Additionally, the rotary vane design minimized pulsations in the air flow.

The air flow system consisted of a factory calibrated rotameter (Fisher and Porter model 5A-25-A) with a metering range of 24-260 1/min of air, two 9.5 mm ball valves (one metering and one bleed), and copper fittings. A thermometer, fixed in a pipe tee, was placed before the rotameter so that the temperature of the incoming air could be recorded; thus corrections to the effects of temperature on the gas flow could be made to the flowmeter readings. A small Bourdon type pressure gauge was installed before the rotameter. Initial experiments showed that the line pressure was less than 0.07 atm. From tabulated values (34) of correction factors for rotameters operating at line pressures greater than ambient, the error in the flowmeter reading at a pressure of 0.07 atm was found to be less than 1%. Thus pressure corrections to flowmeter readings were deemed unnecessary. A small baffled tank was located after the metering valves to eliminate high frequency vibrations in the incoming air.

A flexible, wire supported, polyethylene tube fitted with cuffs was attached from the outlet of the rotameter to the sparger inlet. The tube

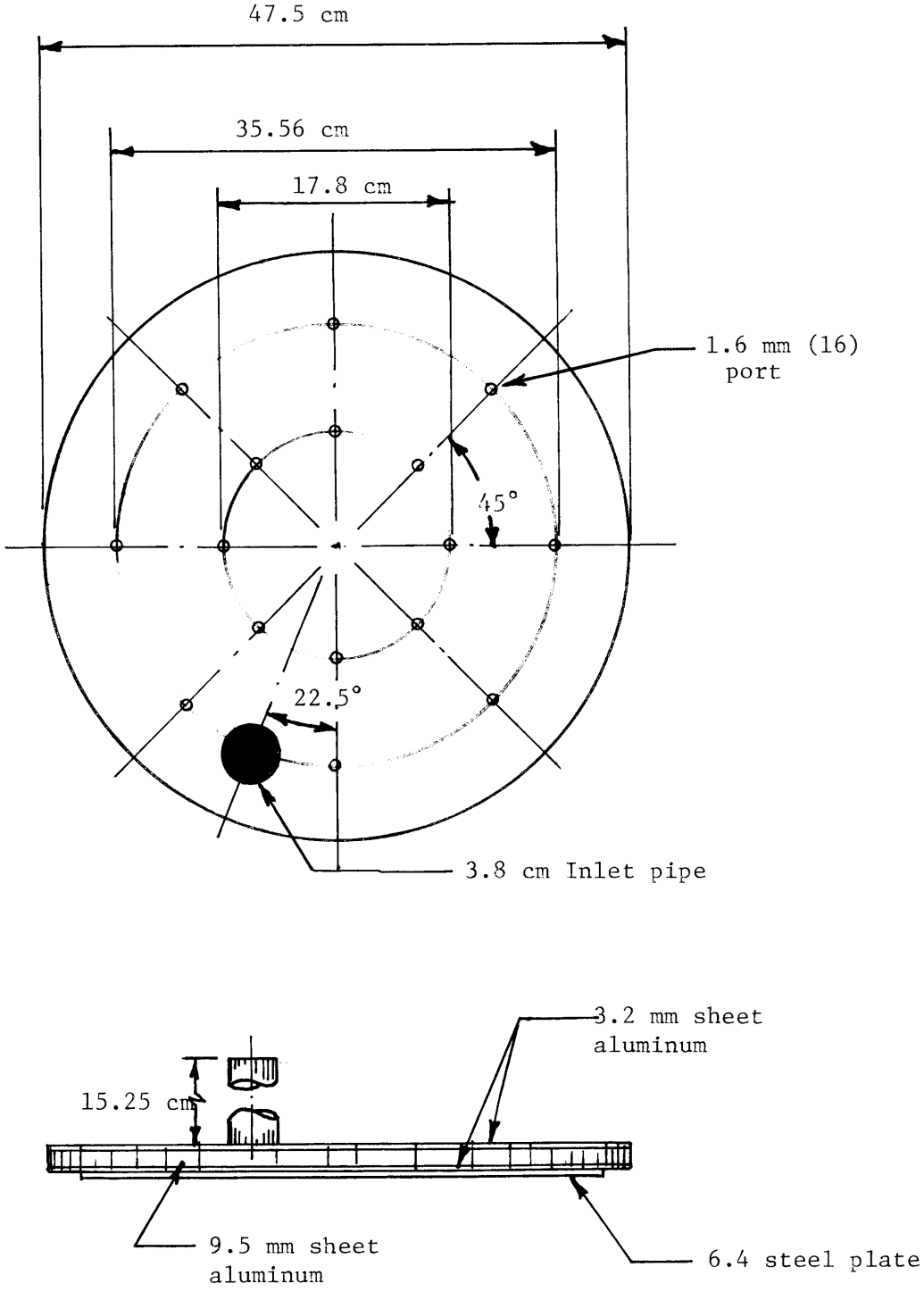

Figure VIII - Details of Sparger Construction

allowed the removal of the sparger between runs. The tube pressure rating was less than 0.34 atm but was adequate because of the low pressure employed.

Prior to the beginning of the experiment, the entire system was checked for air leaks and fittings were tightened where necessary.

IV.B. Procedure

This section includes a description of the methods of making particles and a review of the experimental procedures.

IV.B.1. Particle Manufacture

A total of 109 experimental runs were made during the course of the present work; this required over 260 spherical pellets.

A suitable technique for producing a large number of dimensionally consistent pellets of varying density was developed to meet the needs of this program of study. Particles of benzoic acid ($C_7H_6O_2$, m.p. 122.4°C, ρ = 1.366 gm/cm^3) where cast in spherical 0.958 cm diameter round ball bullet molds supplied by Lee Precision Products Corporation of Hartford, Wisconsin. The acid was first melted in a beaker and then poured into molds which had been chilled with ice. Neutrally buoyant particles with densities corresponding to those of the various solutions were produced through a slush casting process. After the liquid acid was introduced into the molds, solidification was allowed to proceed for a limited period of time. The remaining liquid acid was then shaken from the mold. Since solidification occurred radially from the mold wall, the surfaces of the particles were generally free of defects. Only particles with smooth surfaces were used in the experiments.

Smooth particles were weighed in an analytic balance and grouped according to density. Density differences between solutions and particles were held to within + 1% and - 5%.

Particles were joined into paired and tetrahedrally arranged groupings by holding finished particles in an aluminum fixture and solidifying adjacent surfaces together with a soldering pen.

IV.B.2. Experimental Procedure

Prior to the undertaking of any group of experiments the tank was filled to a depth of 30 cm with approximate volumes of glycerol and distilled water corresponding to the appropriate viscosity to be employed. The solution was mixed for thirty minutes with the sparging apparatus and then allowed to stand for an additional thirty minutes to allow all entrained gas to escape from the liquid. Next, ten samples (10 ml each) were taken from various locations in the tank and weighed in an Ainsworth model 10V analytic balance. An average density was then calculated and used to determine the weight percent glycerol in the system. Solution viscosities were established from tabulated values of viscosity vs. weight percent glycerol (35).

A typical experimental run proceeded in the following manner:

1. Particles (single, pair, andtetrahedral) were weighed in the analytic balance and particle diameters measured with a micrometer (Mitutoyo, model 103-127 accurate to 0.025 mm).

2. The sparger was placed in the tank and the flow rate adjusted to 47, 94, 140 or 188 1/min. (These flow rates were used for all

viscosities.) Sufficient time was allowed for the air temperature to stabilize before a final adjustment was made in the incoming air flow rate. The stabilization time also allowed the gas entrainment to reach a steady level.

3. The bath temperature was measured to within 1/2°C with a thermometer.

4. The particles were next introduced into the agitated liquid with residence times being monitored with stopwatches.

5. Particles were periodically withdrawn from the tank with a basket-type strainer with residence times being subsequently recorded.

6. The particles were first allowed to dry on filter paper before being weighed in the balance. Particle diameters were also noted.

Steps 4-6 were repeated until five or six readings were made. The data were then plotted to yield a weight vs. time curve from which a convective coefficient could be calculated.

The duration of experimental runs averaged from three hours to forty minutes. At the high end of the range of values of Sc measurements were taken at thirty minute intervals. At low values of Sc readings were taken every five minutes.

V. RESULTS

This section presents the data reduction methods used to construct the Brian-Hales correlation and the experimental results accompanied by an analysis of errors.

V.A. Method of Data Evaluation

In order to check experimental data against the Brian-Hales correlation three sets of calculations (one for each parameter Sh, Sc, and Ko) were made.

Sherwood numbers (Sh = h'd/D) were determined from slopes of the particle weight vs. time curves, calculated values of the diffusion coefficient, and measured values of particle diameters.

The convective coefficient h' was calculated from a mass balance on an individual particle:

(change in particle mass) = (mass transferred to bath)

$$\frac{-d}{dt}\,(\text{particle weight}) = h'A(C_s - C_b) \qquad (V.1)$$

here,

h' = convective mass transfer coefficient, cm/sec

A = particle surface area, cm^2

C_s = concentration of solute at the particle surface, gms/cm^3

C_b = concentration of solute in bulk fluid, gms/cm^3

In solving Equation (V.1), it was assumed that $C_b \approx 0$ and that C_s was equal to $\rho_f C_s^*$, the fluid density (ρ_f) times the value of the

solubility limit of the acid (C_s^*). Introducing these changes, Equation (V.1) becomes:

$$\frac{-d}{dt}\ (\text{particle weight}) = h'\ 4\pi R^2\ \rho_f C_s^* \qquad (V.2)$$

or,

$$h' = \frac{\frac{-d}{dt}\ (\text{particle weight})}{4\pi R^2 \rho_f C_s^*} \qquad (V.3)$$

where R = particle radius, cm.

For paired and tetrahedrally arranged groupings of particles, Equation (V.3) was modified to reflect the loss in surface area due to the joined surfaces between particles. In the case of paired particles, the diameters of the particle joints for several pairs was measured with a caliper (Helios Model #V-4 accurate to 0.025 mm); the average value of the joint diameter was found to be 3.45 mm. The particle surface area taken up by the joint was then determined through a simple calculation of the area of a disc (i.e., the effect of the radius of curvature on the area of the joint was assumed to be negligible). It was assumed for tetrahedrally arranged particles that the surface area of a single particle covered by joints to the three adjoining particles was equal to twice that for a paired particle. The weight losses recorded for pairs and tetrahedrals were divided by two or four respectively so that the resulting slope -d/dt (particle weight) represented the mass loss for a single particle of the group.

Thus, for paired and tetrahedrally arranged particles, Equation (V.3) becomes:

$$h' = \frac{\frac{-d}{dt}\ (\text{particle weight})}{(4\pi R^2 - 0.374)\ \rho_f C_s^*} \quad \text{(pairs)} \qquad \text{(V.4)}$$

and,

$$h' = \frac{\frac{-d}{dt}\ (\text{particle weight})}{(4\pi R^2 - 0.748)\ \rho_f C_s^*} \quad \text{(tetrahedrals)} \qquad \text{(V.5)}$$

The fluid density was measured as noted previously. C_s^* can be interpolated from the values given by Harriott and Hamilton (36). However, since these measured values of C_s^* were obtained at 25°C, and the present work was conducted at from 21.5 to 26°C, the measured values were used. Little error was incurred through this approximation. (See Appendix B.)

Diffusion coefficients were calculated with the aid of the Wilke-Chang (37) correlation and the work of Le Bas (38). A complete description of the determination of the diffusion coefficients is given in Appendix C.

The Schmidt number ($Sc = \frac{\nu}{D}$) was determined from the calculated diffusion coefficients and values of viscosity published from the International Critical Tables (35). Because viscosities of the solution varied so strongly with temperature, graphs of viscosity vs. temperature were constructed corresponding to the compositions employed. Accurate values of viscosity could then be read from the graphs. (See Appendix D).

The Kolmogoroff number $Ko = (\frac{\varepsilon d^4}{\nu^3})$ was calculated in the following manner: d was taken as the average of the initial and final diameters for a single particle regardless of the particle grouping, and ν was

determined graphically; ε was calculated based upon a method outlined by Nakanishi et al. (39) which is described below.

Figure IX illustrates schematically a bubble rising in a fluid. Z is equal to the bath height, P_A is equal to the atmospheric pressure, and Z' denotes the distance of the bubble center-line from the datum.

In developing the equations for the energy transfer from the rising gas to the fluid bath the following assumptions are made:

a. interactions between bubbles are neglected,

b. frictional effects are neglected,

c. the gas expands to a volume corresponding to the liquid temperature immediately after being injected into the bath, and

d. the gas behaves ideally.

The work done by a bubble in rising over a distance dZ is taken as equal to the sum of work done by buoyancy forces and the volumetric work:

$$dW = \rho g V dZ' + PdV \qquad (V.4)$$

After some rearrangement, Equation (V.4) becomes:

$$dW = \frac{2nRT}{pg(Z-Z') + P_A} dZ' \qquad (V.5)$$

By integrating Equation (2) between the limits Z'=0 and Z'=Z the work done on the fluid by one bubble is obtained:

$$W = 2nRTLN \left[1 + \frac{\rho gZ}{P_A}\right] \qquad (V.6)$$

If it is assumed that the gas entrs the system at a flow rate of Q(l/min) and that the bubbling stream breaks up into N uniform bubbles

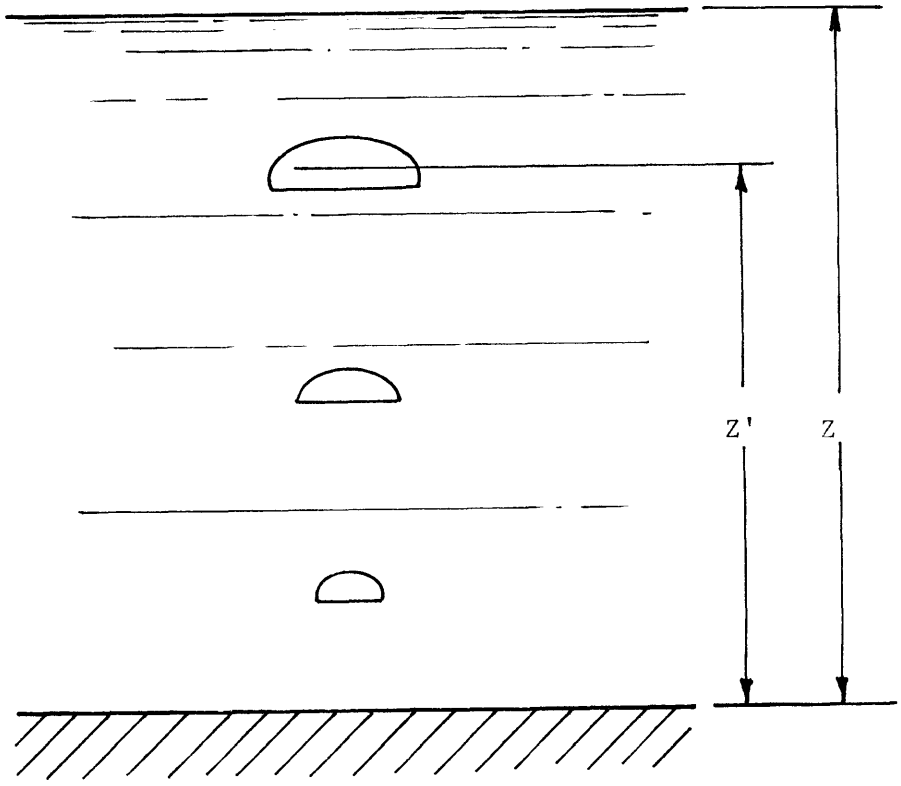

Figure IX - Bubble Rising Through Liquid

per sec the following result is obtained:

$$NW = 1.237 \times 10^{5} (Q)(T)LN[1 + 9.679 \times 10^{-4} \rho Z] \quad (V.7)$$

If Equation (V.7) is divided by the mass of the bath, the power input per unit mass is obtained.

$$\varepsilon = \frac{50.40\ Q\ T}{\rho Z} LN[1 + 9.679 \times 10^{-4} \rho Z] \quad (V.8)$$

where,

ε = power dissipation per unit mass (cm^2/sec^3)

ρ = fluid density (g/cm^3)

T = bath temperature (°K)

Z = bath depth (cm)

The Kolmogoroff number was calculated by the appropriate combination of ε, d, and ν. (Sample calculations are given in Appendix E.)

V.B. Experimental Results

Least square lines were fitted to the data for single particles, paired particles, and tetrahedral clusters so that a comparison could be made for the different types of particles and clusters. The experimental results are shown in Figures X, XI, and XII. (The data is also presented in tabular form in Appendix G.) Equations of the least square lines are given below.

$$\frac{Sh}{Sc^{1/3}} = 0.139\ (Ko^{1/3})^{0.787} \quad \text{single particles} \quad (V.9)$$

$$\frac{Sh}{Sc^{1/3}} = 0.177\ (Ko^{1/3})^{0.761} \quad \text{paired particles} \quad (V.10)$$

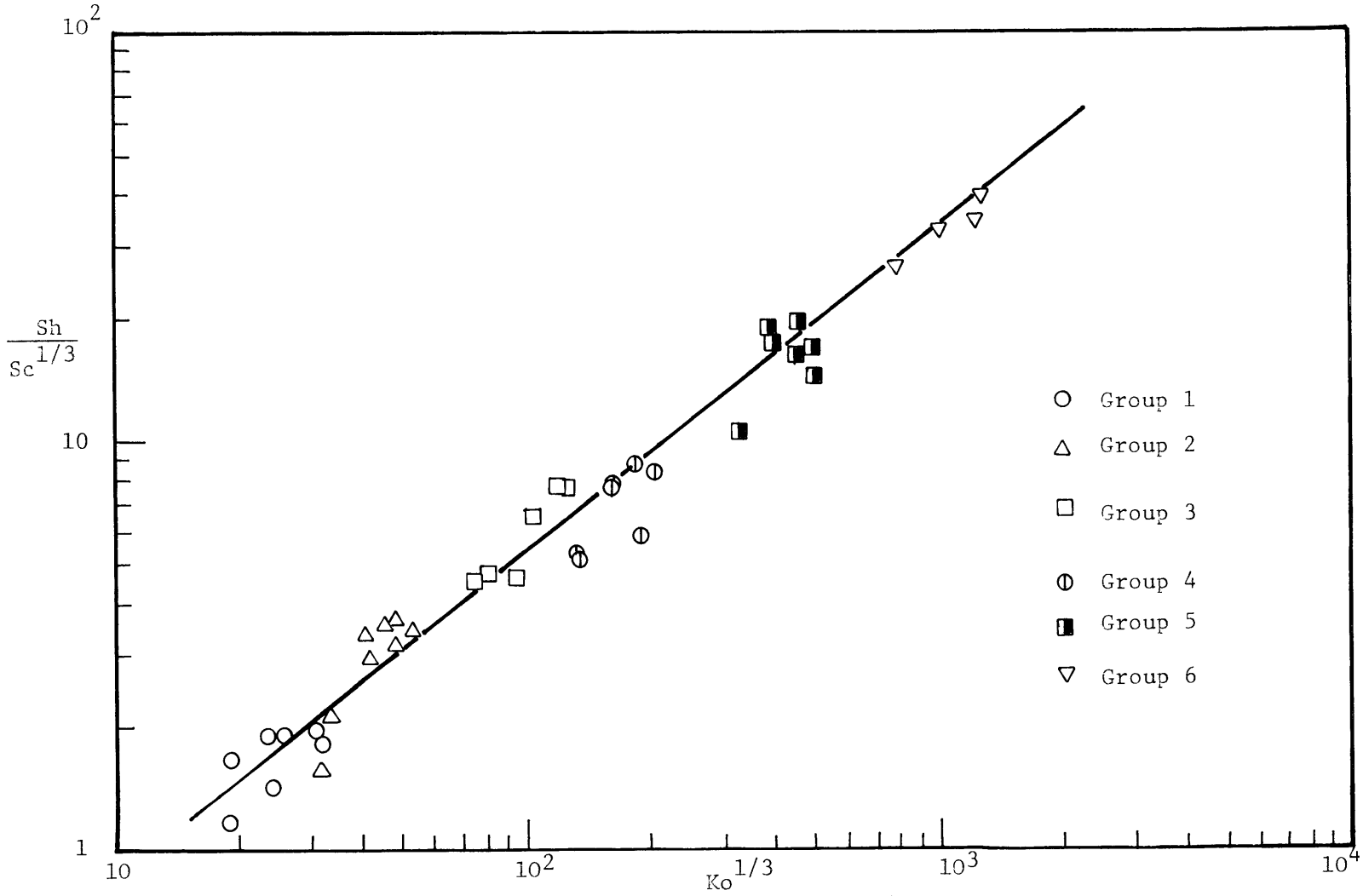

Figure X - Results for Single Particles

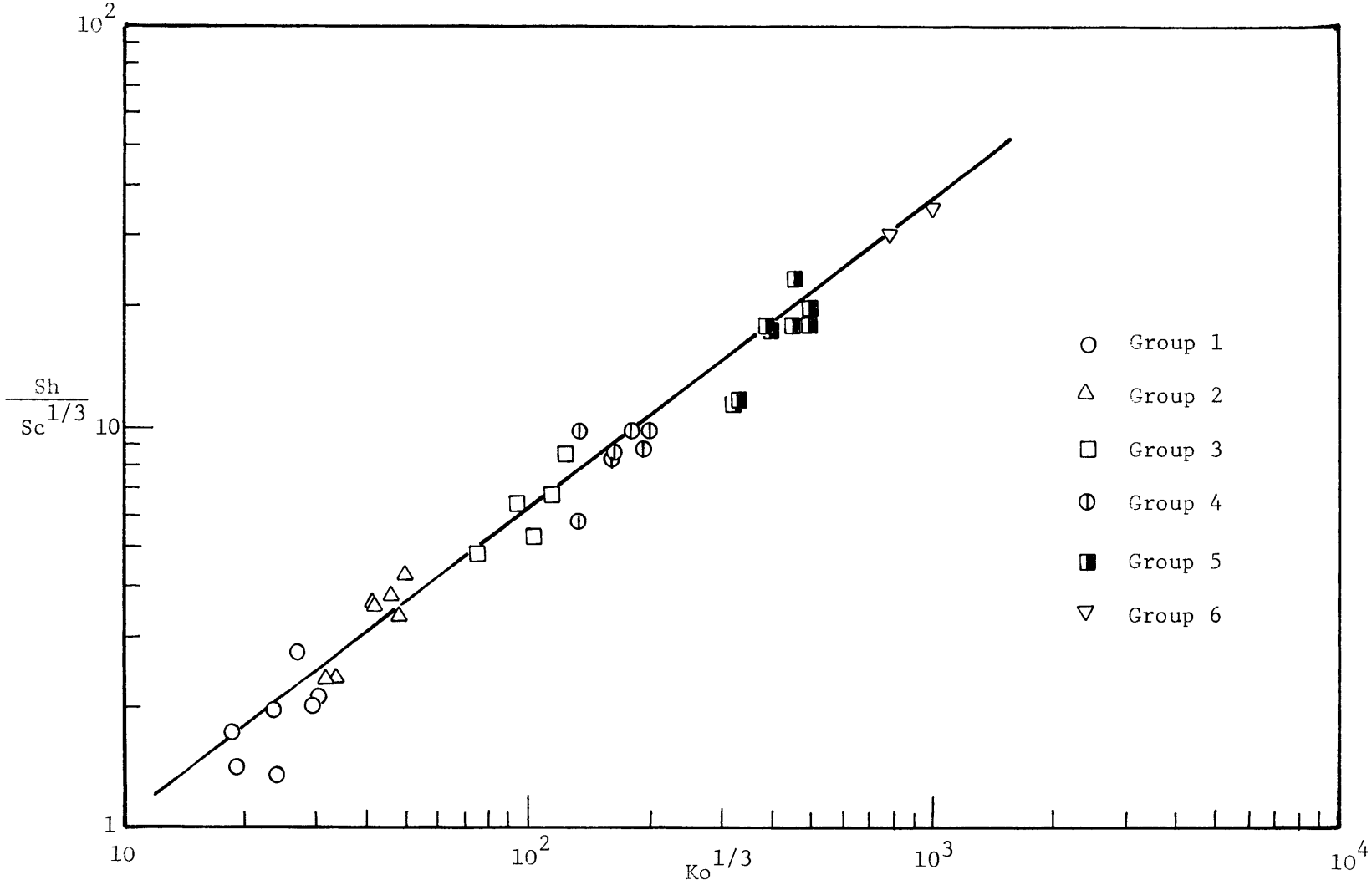

Figure XI - Results for Paired Particles

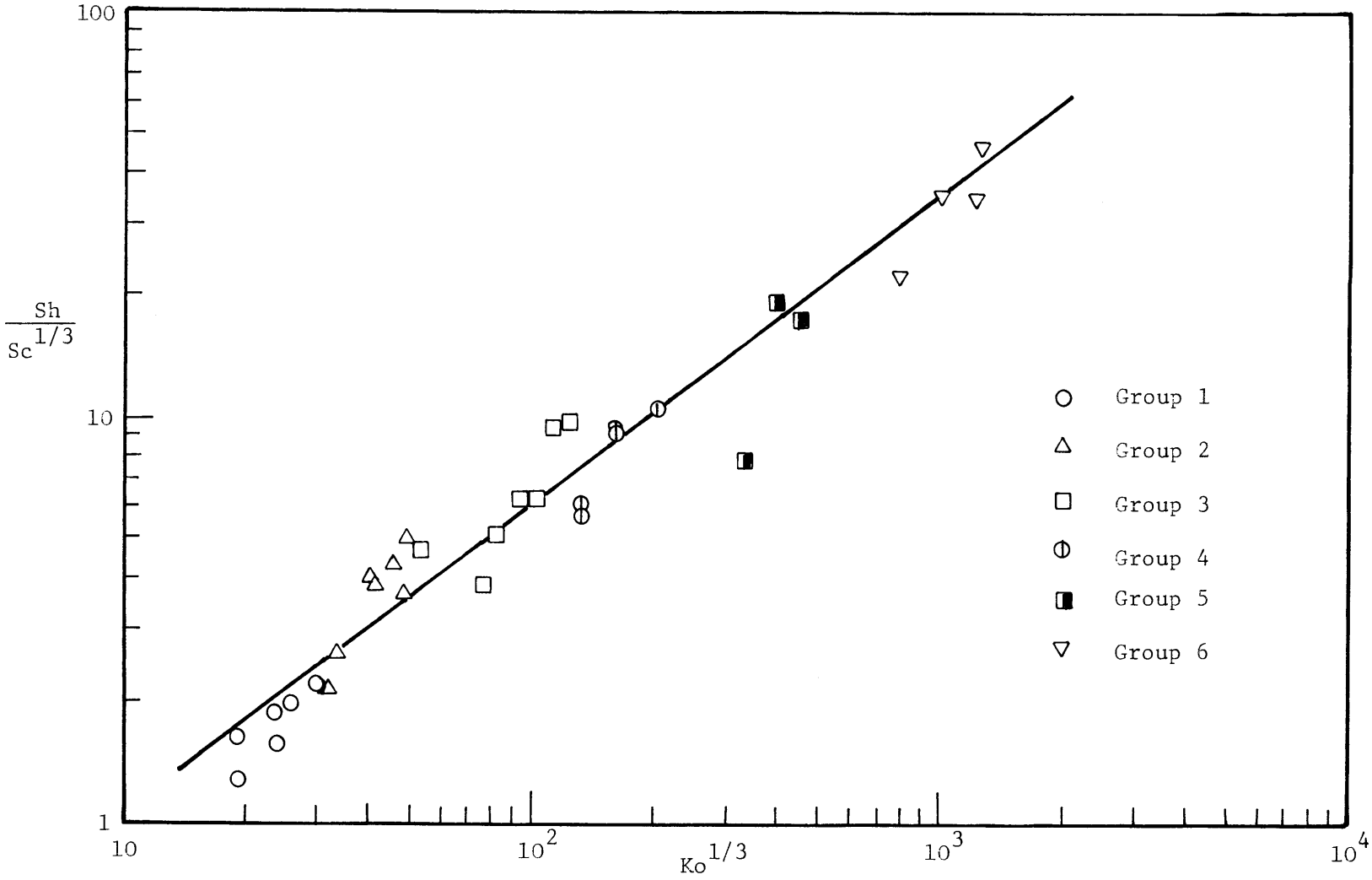

Figure XII - Results for Tetrahedrally Grouped Particles

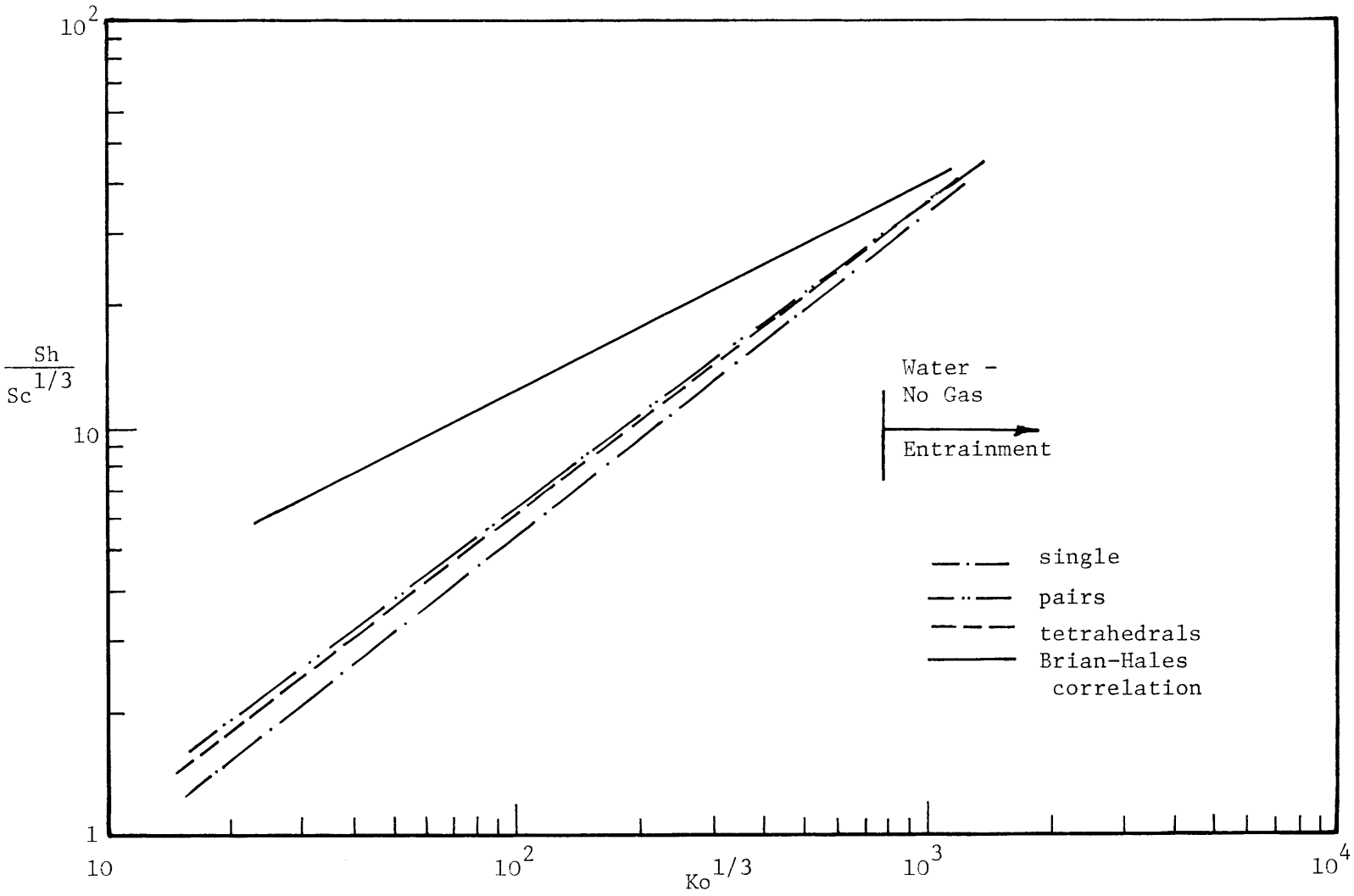

Figure XIII - Brian-Hales Correlation and Correlation Lines of Present Work

$$\frac{Sh}{Sc^{1/3}} = 0.186\ (Ko^{1/3})^{0.752} \qquad \text{Tetrahedrally arranged particles} \qquad (V.11)$$

Figure XIII shows only the correlation lines and the line of the Brian-Hales correlation. As a result of the similarity among the different lines of this study, a single equation can be used to represent the data regardless of the type of particle geometry:

$$\frac{Sh}{Sc^{1/3}} = 0.167\ (Ko^{1/3})^{0.764} \qquad (V.12)$$

or

$$Sh = 0.167\ Ko^{0.255}\ Sc^{0.333} \qquad (V.13)$$

V.C. Analysis of Errors

An analysis of errors for the major parameters and variables was conducted according to the techniques outlined by Mickley et al. (43) and Holman (44). Details of the procedure are given in Appendix F. The analysis is presented in Table III.

Table III - Maximum Error of Variables

Variable/parameter	Maximum % error
d/dt (particle weight)	0.35
ε	6.0
h'	6.13
Sh	11.4
Sc	8.0
$Sh/Sc^{1/3}$	14.1
$Ko^{1/3}$	5.3

VI. DISCUSSION

Preface

The evaluation of the results shown in Figures X, XI and XII must be made not only in light of Kolmogoroff's theory but also through visual observations made during the course of the experiments. The following sections deal with the visual aspects of the work and the displacement to the right of the correlation line of this study relative to the correlation by Brian, Hales and Sherwood (21). The results are finally assessed in terms of their significance to the DRI particle-slag system.

VI.A. Visual Observations

For all experiments in which a solution of glycerol and water was employed, a heavy entrainment of spherical gas bubbles in the liquid was observed. The size of the bubbles was estimated to be between 0.80 and 1.6 mm in diameter. This determination was made through an approximate size comparison between the particles and the entrained bubbles. An estimate of the volume fraction of gas in the system was also made by taking samples of the foamy solution with a 250 ml erlenmeyer flask and recording the volume change after the gas had escaped from the liquid. This procedure was not very accurate but did indicate an entrainment of at least 4% by volume at a flow rate of 188 L/min and about 2% by volume at 47 L/min regardless of viscosity. Since there was no noticeable change in the height of the bath during agiration the level of entrainment was certainly less than 10%; thus, the air/glycerol-water systems formed gas emulsions.

In all cases where entrainment was appreciable the solutions were barely translucent at 47 L/min (i.e., bubble columns could still be seen) and were completely opaque with a whitish appearance at a flow rate of 188 L/min.

The general flow pattern of the system is shown in Figure XIV. The pattern was deduced from the motion of entrained bubbles which acted as tracers. Figure XIV-A shows a sectional view of the tank where bubble columns can be seen curving inward toward the center of the tank. The rising gas together with the wall boundaries produced an annulus effect (shown in Figure XIV-B) which has also been observed for bubble columns (42).

Particles were seen following the annulus pattern. Because particles were neutrally buoyant in all cases, direct interaction of particles with bubbling chains from the sparger also occurred. Particles in the glycerol-water solutions developed layers of bubbles adhering to the surfaces of the pellets. It was estimated that more than 50% of the surface of an individual particle was covered by a layer of small bubbles (0.8 mm in dia.) irrespective of viscosity of the liquid. The coverage of bubbles on the surfaces of particles was the same (i.e., $> 50\%$) regardless of the solution viscosity and flow rate of air into the system. The bubble layers were seen to be swept away as particles interacted with the bubble columns. (This observation was only made at a flowrate of 47 L/min.)

Experiments conducted with pure water failed to show any indication of entrainment save for a few large bubbles ($\sim$ 5 mm dia.) which could

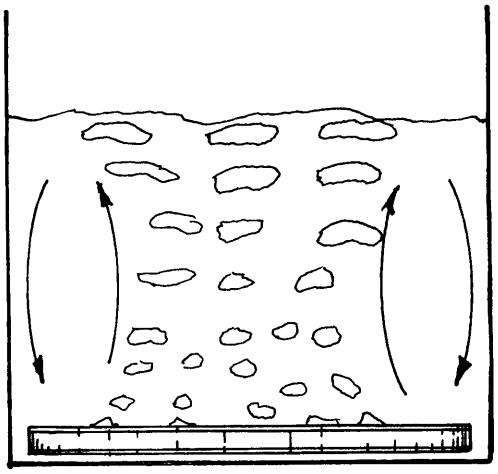

A. Section

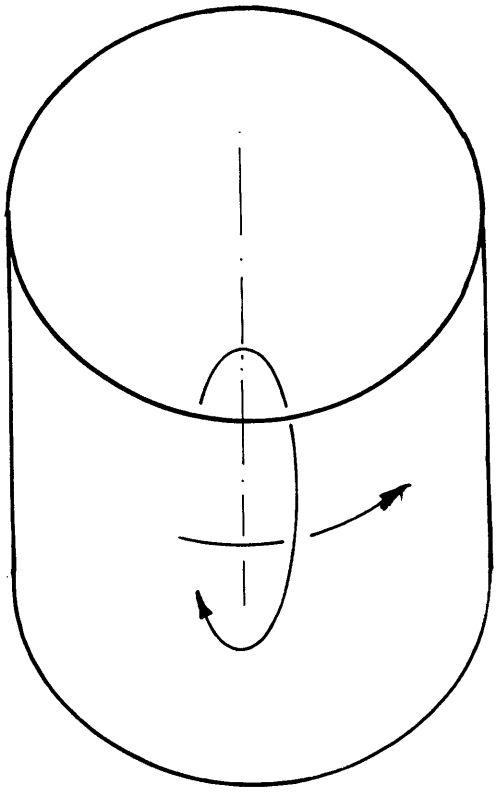

B. Flow Annulus

Figure XIV - Flow Pattern in Laboratory Model

be seen at the tank wall. No adherence of bubbles on the surfaces of particles was observed. As in the case of the high viscosity solutions, particles tended to move in the flow annulus with direct particle-bubble column interactions also taking place.

VI.B. Interpretation of the Displacement of the Experimental Correlation from the Brian-Hales Correlation

The displacement of the experimental correlations from the Brian-Hales correlation (see Figure XIII) may be the result of three factors:

1. The adherence of bubbles on the surfaces of particles,
2. a possible increase in the liquid viscosity due to the presence of entrained gas, or
3. the convective eddies falling outside of the universal equilibrium range of the energy spectrum.

Bubbles adhering on the surfaces of particles could lower dissolution rates through a reduction in surface area open for mass transfer. This effect would be interpreted in Figure XIII as a decrease in values of the Sherwood number for the case of gas entrainment in the liquid phase relative to those predicted by the Brian-Hales correlation.

The importance of this factor is diminished when the results for the water-glycerol solutions are compared with those for pure water; if the adherence of bubbles actually resulted in a lowering of particle dissolution rates, then, contrary to the data of Figure XIII, results for the water experiments would lie above the least square lines for the high viscosity solutions.

The second factor involves an increase in viscosity due to the presence of finely entrained gas in the liquid. Sibree (40) investigated the viscosities of froths (i.e., foams and gas emulsions) and found that even a small volume of highly dispersed gas can result in a large increase in viscosity. He proposed that an effective viscosity could be calculated according to the equation:

$$\nu_E = \nu_o \frac{1}{1 - \sqrt[3]{\phi}} \qquad \text{(VI.1)}$$

where

ν_E = effective viscosity

ν_o = molecular viscosity

ϕ = volume fraction of gas

If the above relation is used to calculate an effective viscosity for the water-glycerol solutions, the ratio ν_E/ν_o is equal to 1.52 assuming a value of ϕ equal to 0.04. Effective viscosities substituted into the Kolmogoroff number, where ν appears to the third power, would result in a major shift of the lines of Figure XII to the left, towards the Brian-Hales correlation. (The significance of ν_E on the group $Sh/Sc^{1/3}$ would be small in comparison to the effect on $Ko^{1/3}$ since viscosity is taken to the one third power in the ordinate group.) The factor seems unimportant because of the results of the water experiments. Although gas may be entrained in the water-glycerol solutions, the viscosities may not be affected to the extent predicted by Equation (VI.1).

It is also improbable that gas entrainment could affect the power input, again because of the water model data. Additionally, any impact of the variable ε is significantly reduced by the one third exponent of the Kolmogoroff number.

The most plausible explanation for the displacement of the experimental results is that the eddies which are primarily responsible for convective transfer possess wavenumbers less than k_e and are consequently non-isotropic. If this is the case the rates of dissolution will depend upon the method of agitation and the dimensions of the liquid system.

Observations of dissolution for grouped arrays of particles revealed that all areas of the grouped surfaces evidenced equal rates of attack. The only way that the particle clusters could be dissolved in an even manner would be through the action of small isotropic eddies. The eddies contributing to particle dissolution fall into a wide range of wavenumbers: eddies which are on the order of the particle diameter may contribute only in part to the overall dissolution rate with smaller isotropic eddies enhancing mass transfer. The importance of the particle diameter factor can be established through experiment. A discussion of the experimental method is given in Chapter VIII.

VI.C. Significance of the Experimental Results to the DRI-Particle Slag System

It was necessary to determine the influence of the Sc on Sh, the effect of gas entrainment, the importance of particle agglomeration, and the effect of particle-bubble interactions in order to establish

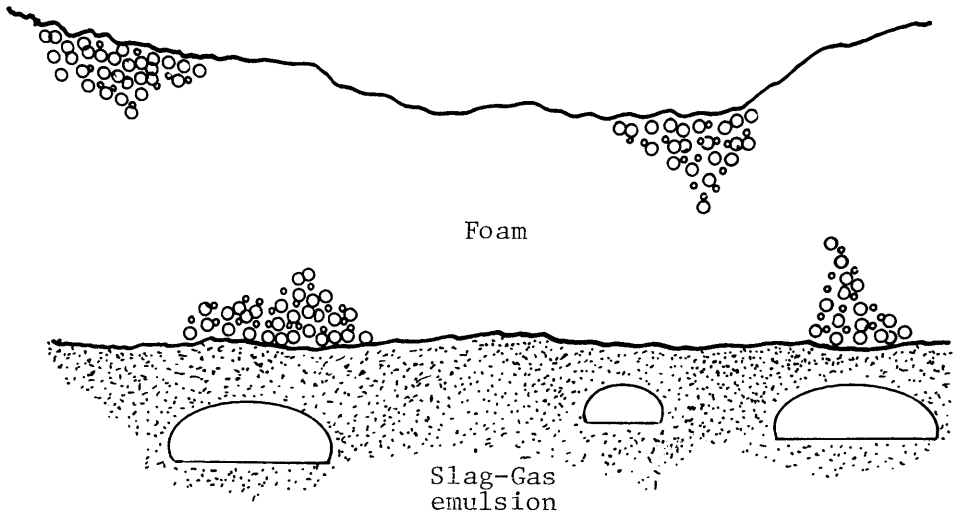

Figure XV - Foaming of Slag Pool

if Brian-Hales correlation could be applied to the particle-slag system.

Inspection of Figure XIII for the entire range of viscosities and Schmidt numbers tested shows that all data may be correlated by one relation. Because deviations are absent (e.g., bands of data corresponding to different values of Sc did not appear) it may be assumed that the correlation is not strongly dependent on the Schmidt number; the insensitivity of the results is particularly encouraging with regard to the potential limitations of the mass transfer analogy discussed earlier.

Gas entrainment in the liquid phase produces no observable effect. The primary difficulty in extending the results for the model gas emulsions to the industrial problem is that under normal operating conditions most electric furnace slags double in volume under the action of the carbon boil (4). Thus the slags may be through of as foams (i.e., entrainment >10%) and not as emulsions of gas and liquid. However, foaming may occur on the surface or slags with gas still entrained in the remaining liquid (see Figure XV). If this is the case, the actual melting of DRI particles would occur in the slag-gas emulsion. This would seem likely inasmuch as a doubling of gas volume would correspond to a decrease of 50% in the slag density. Particles of DRI, which have a density equal to that of liquid slags, would easily drop though the foam and into the emulsion.

Since the data of single, paired, and tetrahedrally arranged particles can all be correlated by one relation, the effect of agglomeration on the <u>local</u> rates of transport is negligible .

It has been observed (4) that clumps or islands of DRI particles melt more slowly than individual ones. From the results of this study it is evident that any decrease in heat transfer is the result of a decrease in the ratio of convective surface area to particle group mass.

The qualitative effect of particles colliding with large bubbles rising through the fluid was seen to be a removal of bubbles attached to the surfaces of particles in cases where water-glycerol solutions were utilized. Particle-bubble interactions also occurred in the experiments in which pure water was employed; in these experiments, layers of bubbles covering the surfaces of particles were absent. Since the results for all experiments lie on one line and are correlated through the variables ε and ν, collisions between large bubbles and particles do not result in a transfer mechanism different from a slip velocity mechanism as the dominant means of heat or mass transfer.

As noted in the discussion of particle diameter, the lack of geometric similarity between the model and the electric furnace slag pool is potentially the most significant restriction to the extension of the experimental results to the industrial system. The effect of system boundaries on rates of dissolution or heat transfer can also be determined through further experiments. Chapter VIII presents a discussion of suggestions for further work in this area.

VII. SUMMARY AND CONCLUSIONS

The Brian-Hales correlation has been tested for application to the melting of DRI pellets immersed in turbulent, bubble stirred, electric furnace slags through a low temperature model in which spherical particles of benzoic acid were dissolved in water and solutions of glycerol and water stirred with compressed air; agitation of solutions of glycerol and water resulted in a heavy entrainment of fine gas bubbles. The results of the study show that the data for single and grouped configurations of particles lie on one correlation line although values of $(Sh/Sc^{1/3})$ are approximately one order of magnitude below the Brian-Hales correlation for values of Ko less than 40.

The major conclusions which may be drawn from the experimental results are:

1. The presence of entrained gas, and the adherence of bubbles on the surfaces of particles, produces no major effects on the rates of particle mass transfer;

2. The Schmidt number does not affect the value of the Sherwood number over a range in values of Sc from 10^3 to 10^6;

3. The rates of particle heat or mass transfer are independent of particle clustering.

It must be emphasized that the extension of the grouped particle experiments to large clumps of particles (i.e., more than four particles) must be viewed with caution. Based on theoretical grounds, the results of this study cannot be applied to large groupings of particles.

VIII. SUGGESTIONS FOR FURTHER WORK

Further research should be directed toward determining if non-isotropic eddies influence heat transfer rates of particles of DRI. Specifically, two types of experiments should be conducted. First, dissolution experiments employing particles of benzoic acid, and the same tank dimensions, viscosities, and particle diameter as used in the present work should be undertaken but with an impeller as the source of agitation. If non-isotropic eddies influence heat or mass transfer the results for impeller agitation should lie above or below the correlation lines of this study. Second, the flexible slag-metal interface should be modeled in a future study. The modeling may be achieved with a layered mercury bath and glycerol-water system. The experiments should be conducted with as large a vessel as practical. The comparison of the results of such experiments with those of the present study would indicate if a non-geometric scaling is significant to the determination of particle heat or mass transfer rates.

APPENDIX A

Calculation of the Kolmogoroff Number for the Electric Furnace

The range in values of Ko for a 200 t electric furnace was calculated from the furnace modeling parameters and variables given in Table I, and Equation (V.7).

The flowrates of CO gas through the slag layer range from

$$(4.20 \frac{mol}{sec})(22.4 \frac{L}{mol})(60 \frac{sec}{min}) = 5644.80 \frac{L}{min}$$

to

$$(8.40 \frac{mol}{sec})(22.4 \frac{L}{mol})(60 \frac{sec}{min}) = 11289.60 \frac{L}{min}$$

The mass of the slag pool was calculated to be

$$\pi (R_{furnace})^2 (Z)(\rho_s) = \text{mass of slag}$$

$$\pi (\frac{724}{2})^2 (30)(3.6) = 4.446 \times 10^7 \text{ grams}$$

By substituting a slag temperature of 1600°C and the CO flowrates given above into Equation (V.7), and dividing the expression by the mass of the slag pool, a range in values of ε was obtained:

$$\varepsilon = \frac{1.237 \times 10^5 (5644.80)(1600 + 273) LN[1 + 9.679 \times 10^{-4})(3.6)(30)]}{4.446 \times 10^7}$$

$$= 2.924 \times 10^3 \text{ cm}^2/\text{sec}^3$$

and

$$\varepsilon = \frac{1.237 \times 10^5 (11289.60)(1600+273) LN\ [1+9.679 \times 10^{-4} (3.6)(30)]}{4.446 \times 10^7}$$

$$= 5.849 \times 10^3 \text{ cm}^2/\text{sec}^3$$

The values of ε given above were then substituted into the Kolmogoroff number:

$$Ko^{1/3} = \left(\frac{\varepsilon d^4}{\nu^3}\right)^{1/3}$$

$$\left(\frac{2.924 \times 10^3 \ (1.2)^4}{(0.57)^3}\right)^{1/3} = 40.31$$

and

$$\left(\frac{5.849 \times 10^3 \ (1.2)^4}{(0.57)^3}\right)^{1/3} = 31.99$$

Although the range in values of $Ko^{1/3}$ calculated from Table I range from 30 to 40, actual furnace CO evolution rates may fall slightly outside of this range (41). Thus, for the present study, values of $Ko^{1/3}$ ranging as low as 20 were used.

APPENDIX B

Solubility of Benzoic Acid in Solutions of Glycerol and Water

Values of the solubility of benzoic acid in water and solutions of glycerol and water are shown in the graph of Figure XVI. The values of the solubilities at 25°C were taken from the study of Harriott and Hamilton (36). The solubilities at 35°C and 15°C were calculated by Wadia (31) with the Clausius-Clapeyron equation; these values are shown for comparison. The present work was conducted at from 21.5 to 26°C and the values of C_s^* were assumed to be equal to those at 25°C. From Figure XVI it is evident that a maximum temperature difference of -3.5°C will affect the values of C_s^* by only about 5% if values are interpolated between the solubility lines.

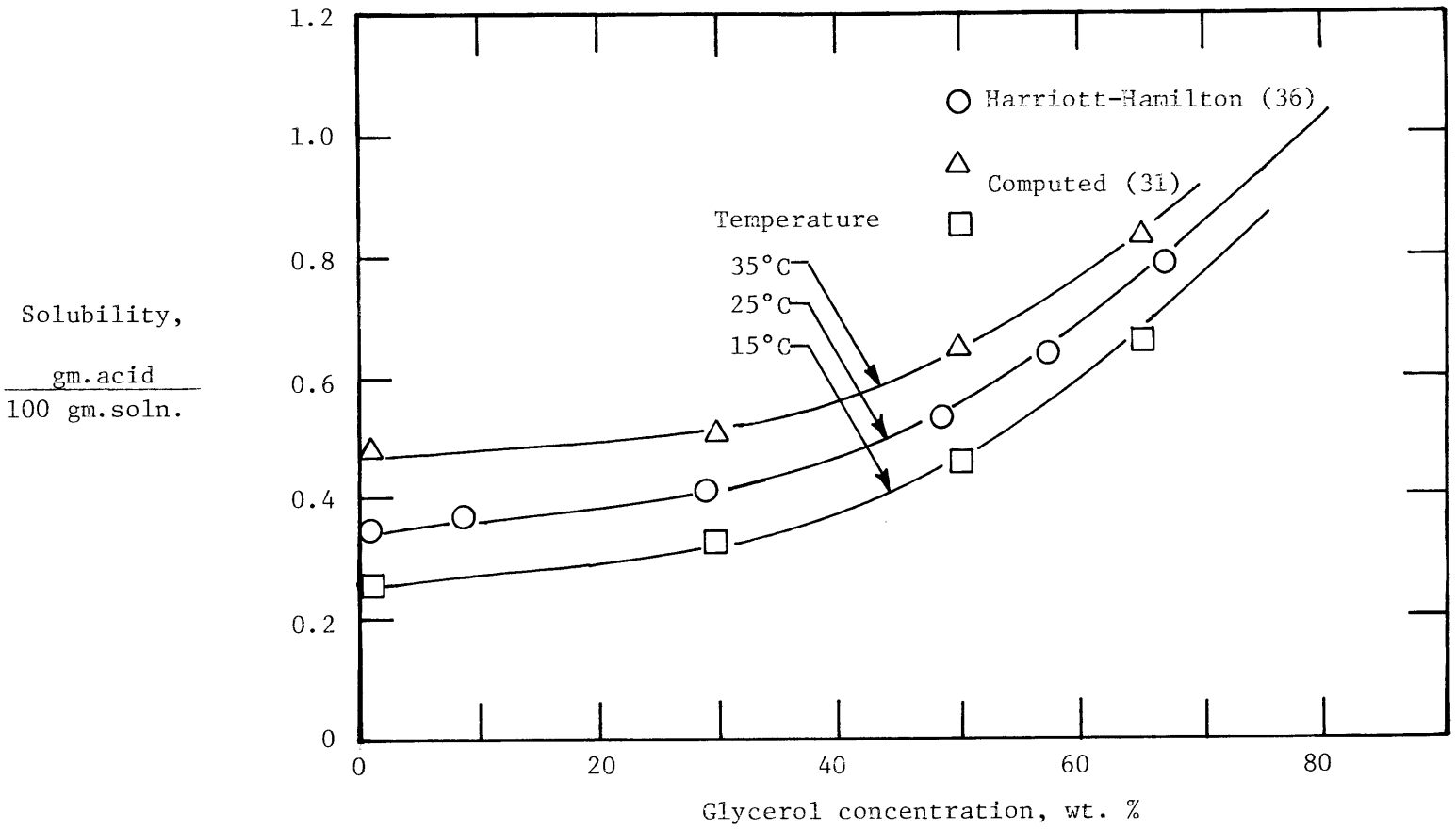

Figure XVI - Solubility of Benzoic Acid in Solutions of Glycerol and Water

APPENDIX C

DIFFUSION COEFFICIENTS

Diffusion coefficients for benzoic acid in water and glycerol-water solutions were calculated with the Wilke-Chang correlation (37). The relation correlates D to the solute molal volume, the molecular weight of the solvent, the solution absolute viscosity, and the fluid temperature.

$$D = 7.4 \times 10^{-8} (X.M)^{1/2} T/\mu V^{0.6} \qquad (C.1)$$

where,

D = solute diffusivity, cm^2/sec

X = association parameter of the solvent

M = molecular weight of the solvent

T = solvent temperature, °K

μ = absolute viscosity of solvent, c.p.

V = solute molal volume at the normal boiling point, cm^3/g mol

The association parameter was taken equal to 2·6. The solute molal volume of benzoic acid given by Le Bas (38) as 126.9 cm^3/g mol

APPENDIX D

Viscosities of Glycerol-Water Solutions

Viscosities of the glycerol-water solutions at various temperatures were determined from Figure XVII. The graph was constructed from the values of viscosity vs. composition given in the International Critical Tables (35).

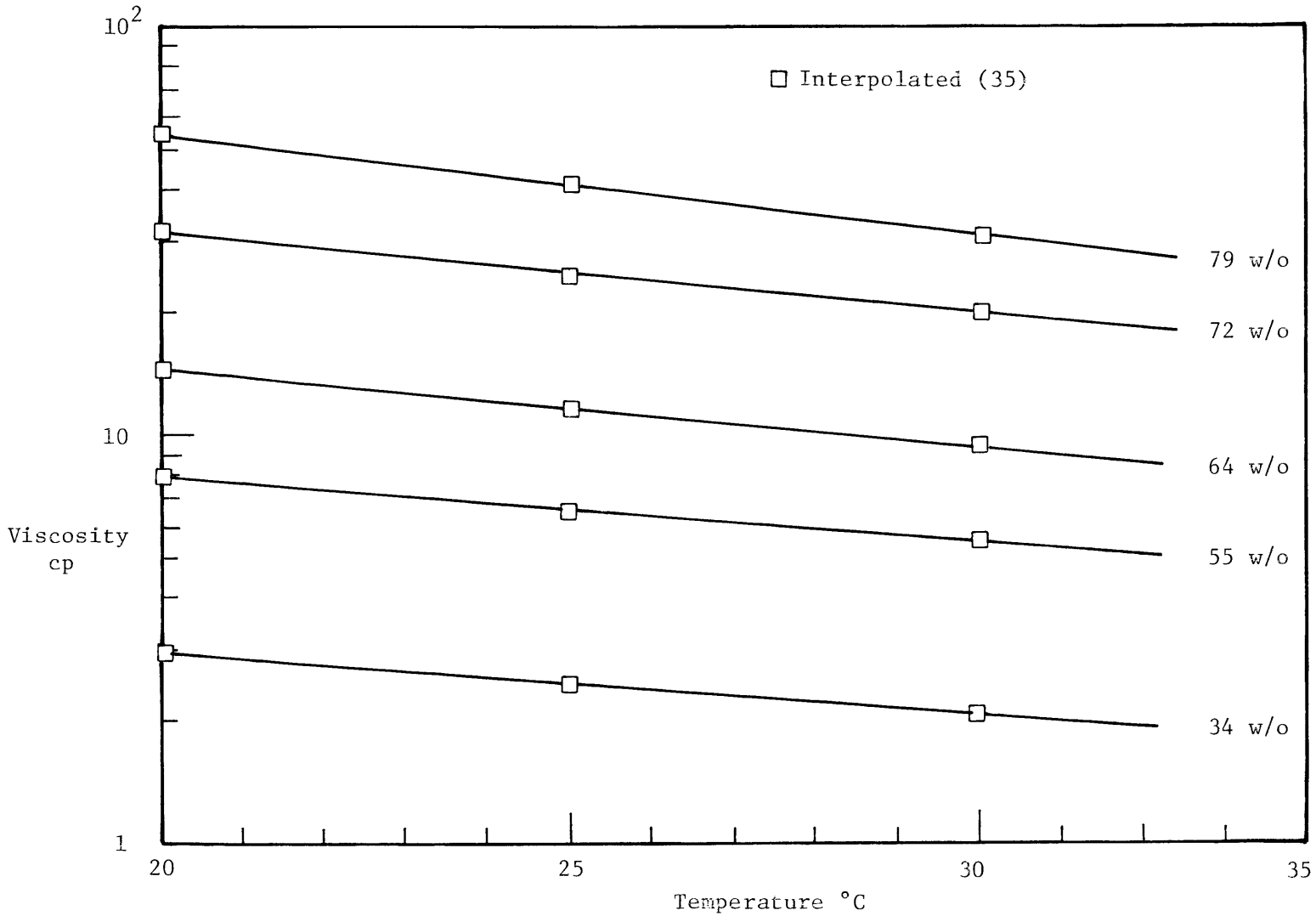

Figure XVII - Viscosities of Glycerol-Water Solutions

APPENDIX E

Sample Calculations

During the course of an experiment the following measurements and experimental conditions were recorded:

1. particle weight recorded over time,
2. initial and final particle diameters,
3. flowrate,
4. bath temperature,
5. incoming air temperature,
6. bath depth, and
7. fluid density

Figure XVIII illustrates the particle weight vs. time plot of a typical run for a single particle. A least-square analysis of these data yields a slope of -1.888×10^{-6} gm/sec. The average of the initial and final particle diameters for this run was found to be 0.944 cm. The fluid density was 1.199 gm/cc and C_s^* was found from Figure XVI to equal 1 gm/100 gm soln. Substitution of these values into Equation (V.3) gives

$$h' = \frac{(-1.888 \times 10^{-6})}{4\pi(\frac{0.944}{2})^2 (1.199)(\frac{1}{106})} = 5.625 \times 10^{-5} \text{ cm/sec}$$

The value of D calculated from Equation (C.1)was 2.717×10^{-7} cm^2/sec.

The Sherwood Number was calculated from the above values of h', d, and D.

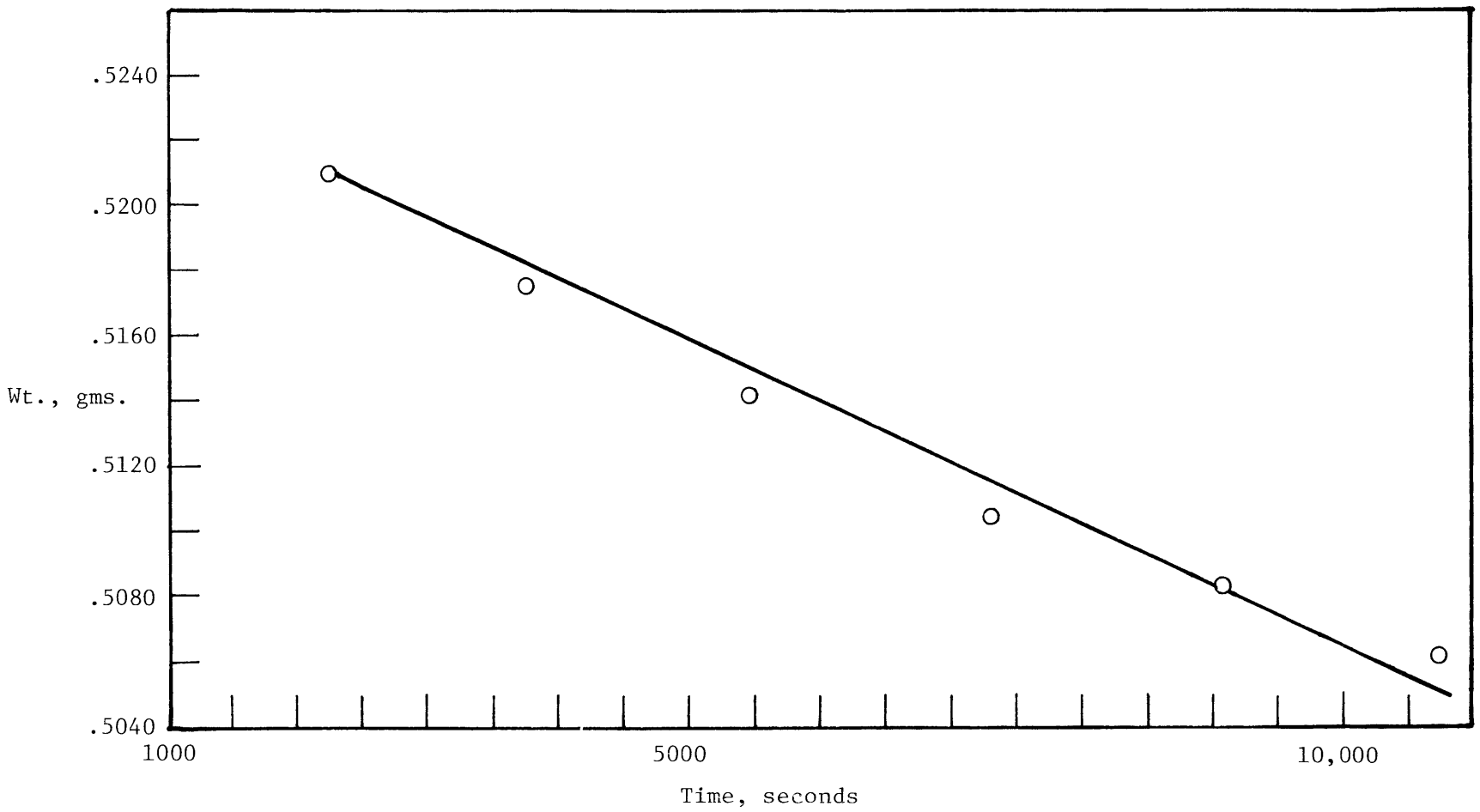

Figure XVIII - Particle Weight vs. Time for Run #11-S

$$Sh = \frac{h'd}{D} = \frac{(5.625 \times 10^{-5})(0.944)}{2.717 \times 10^{-7}} = 195.44$$

The Schmidt number wascalculated from D and the viscosity for a 79 w/o solution at a temperature of 22°C:

$$Sc = \frac{\nu}{D} = \frac{\frac{0.499}{1.199}}{2.717 \times 10^{-7}} = 1.532 \times 10^{6}$$

Thus, the group $(Sh/Sc^{1/3})$ becomes:

$$\frac{Sh}{Sc^{1/3}}) = \frac{195.44}{(1.532 \times 10^{6})^{1/3}} = 1.70$$

The flowrate was set at a reading of 47.19 L/min. The temperature of the incoming air was found to be 29°C. Since the air temperature was not 21°C (for which the Rotameter was calibrated) the operating air temperature was multiplied by a correction factor of 0.985 (34).

For a bath depth of 35.66 cm and the flowrate given above, the power dissipation was determined by Equation (V.8) to be:

$$\varepsilon = \frac{50.40(0.985 \times 47.19)(22 + 273)}{(1.199)(35.66)} LN[1 + 9.679 \times 10^{-4}(1.199)(35.66)]$$

$$= 6.554 \times 10^{2} \text{ cm}^2/\text{sec}^3$$

The value of $Ko^{1/3}$ was then determined:

$$Ko^{1/3} = (\frac{\varepsilon d^4}{\nu^3})^{1/3}$$

$$Ko^{1/3} = (\frac{(6.554 \times 10^{2})(0.944)^4}{(0.416)^3})^{1/3}$$

$$Ko^{1/3} = 19.34$$

Calculations for paired and tetrahedrally arranged particles were carried out in a way similar to that outlined above but with Equations (V.4) and (V.5) replacing Equation (V.3).

APPENDIX F

ANALYSIS OF ERRORS

An analysis of the errors in the major parameters and variables of the study was conducted following the procedures given by Mickley et al (43) and Holman (44). The procedures are outlined below.

If a dependent variable Q is a function of several independent variables qa, qb, ..., qn, which can be represented as

$$Q = qa^{a}\ qb^{b}\ \ldots.\ qn^{n} \qquad \text{(F.1)}$$

Then the maximum error in Q resulting from the errors in the individual variables qa, qb ... qn is

$$\frac{\Delta Q}{Q} = a\ \frac{\Delta qa}{qa} + b\ \frac{\Delta qb}{qb} + \ldots. + n\ \frac{\Delta qn}{qn} \qquad \text{(F.2)}$$

The maximum percent error in the calculated experimental variables (e.g., ε, Sh, Ko, etc.) can be determined with the aid of Equation (F.2).

1. $\frac{d}{dt}$ (particle weight)

$$\frac{\frac{\Delta d}{dt}\ (\text{particle weight})}{\frac{d}{dt}\ (\text{particle weight})} = \frac{\Delta(\text{particle weight})}{(\text{particle weight})} + \frac{\Delta t}{t} \qquad \text{(F.3)}$$

The error in the particle weight measurement was $\pm$ 0.0001 gram. The error in the time readings was $\pm$ 1 sec. For a particle weighing 0.50 grams and a time interval of 5 minutes the error in the value of the particle dissolution rate becomes:

$$\frac{\frac{\Delta d}{dt}\ (\text{particle weight})}{\frac{d}{dt}\ (\text{particle weight})} = \frac{0.0001}{0.5} + \frac{1}{300}$$

$$= 0.0002 + 0.0033$$

$$= 0.0035 \text{ or } 0.35\%$$

2. ε

$$\varepsilon = \frac{50.40\ (Q)\ T}{\rho Z} \text{ LN } [1 + 9.679 \times 10^{-4}\ \rho Z] \qquad (V.8)$$

Before evaluating the error in ε, it will be useful to compare the magnitudes of the errors contributed by the independent variables Q, T, ρ, and Z.

$$\frac{\Delta Q}{Q} = 0.06$$

$$\frac{\Delta T}{T} = 0.0017$$

$$\frac{\Delta \rho_f}{\rho_f} = 0.0026$$

$$\frac{\Delta Z}{Z} = 0.0085$$

By a comparison of the errors listed above it is evident that the error in the flowrate Q is the most significant. Thus

$$\frac{\Delta \varepsilon}{\varepsilon} \approx \frac{\Delta Q}{Q} = 0.06$$

3. h'

$$h' = - \frac{\frac{d}{dt} \text{(particle weight)}}{\pi d^2 \rho_f C_s^*} \tag{V.3}$$

$$\frac{\Delta h'}{h'} = \frac{\frac{\Delta d}{dt} \text{(particle weight)}}{\frac{d}{dt} \text{(particle weight)}} + 2\frac{\Delta d}{d} + \frac{\Delta \rho_f}{\rho_f} + \frac{\Delta C_s^*}{C_s^*} \tag{F.4}$$

The particle diameter was measured to within 0.025 mm for 0.958 cm particles. The error in C_s^* was already noted to be 5%. The largest error in C_s^* resulted from reading the values from the graph. The accuracy of the values given by Harriott and Hamilton (36) is $\pm$ 1.65%.

$$\frac{\Delta h'}{h'} = 0.0035 + 2(0.0026) + 0.0026 + 0.05 = 0.0613$$

4. Sh

$$Sh = \frac{h'd}{D}$$

$$\frac{\Delta Sh}{Sh} = \frac{\Delta h'}{h} + \frac{\Delta d}{d} + \frac{\Delta D}{D} \tag{F.5}$$

The error in the values of D calculated from Equation (C.1) is 5% (31).

$$\frac{\Delta Sh}{Sh} = 0.0613 + 0.0026 + 0.05 = 0.114$$

5. Sc

$$\frac{\Delta Sc}{Sc} = \frac{\Delta \nu}{\nu} + \frac{\Delta D}{D} \tag{F.6}$$

Errors in viscosity arose from the reading of values of Figure XVII. The error is assumed to be 3%.

$$\frac{\Delta Sc}{Sc} = 0.03 + 0.05 = 0.08$$

6. $\frac{Sh}{Sc^{1/3}}$

The error in the ordinate group is

$$\frac{\frac{\Delta Sh}{Sc^{1/3}}}{\frac{Sh}{Sc^{1/3}}} = \frac{\Delta Sh}{Sh} + \frac{1}{3}\frac{\Delta Sc}{Sc} = 0.114 + \frac{1}{3}(0.08) = 0.141 \qquad (F.7)$$

7. $Ko^{1/3}$

The error in the Kolmogoroff number was determined to be:

$$\frac{\Delta\ Ko^{1/3}}{Ko^{1/3}} = \frac{1}{3}\frac{\Delta\varepsilon}{\varepsilon} + \frac{4}{3}\frac{\Delta d}{d} + \frac{\Delta\nu}{\nu} = \frac{1}{3}(0.06) + \frac{4}{3}(0.0026) + \qquad (F.8)$$

$$(0.03) = 0.053$$

APPENDIX G

Tabulation of Data

Note: S = single T = tetrahedral

P = pair

Group 1

79 w/o glycerol

ν = 41.6 c.s.

Z = 35.66 cm

ρ = 1.199 gm/cc

C_s^* = 1 gm/100 gm soln.

Run #	Dissolution rate x 10^{-6} gm/sec			Particle diameter cm			Flow rate L/min	Bath Temp., °C
	S	P	T	S	P	T		
11	1.888	1.683	1.304	0.944	0.952	0.946	46.30	22
12	2.096	1.922	1.547	0.944	0.952	0.948	92.16	22
13	2.096	2.690	1.556	0.946	0.950	0.946	135.92	21.5
14	2.184	1.959	1.814	0.950	0.950	0.946	180.77	22
15	1.325	1.377	1.052	0.944	0.950	0.952	46.08	22
16	1.584	1.341	1.279	0.950	0.958	0.946	91.72	22
18	1.919	2.121	1.813	0.944	0.950	0.946	180.77	22.5

Group 2

72 w/o glycerol

ν = 23.7 c.s.

Z = 35.97 cm

ρ = 1.1793 gm/cc

C_s^* = 0.88 gm/100gm soln.

Run #	Dissolution Rate x 10^{-6} gm/sec			Particle diameter cm			Flow rate L/min	Bath Temp.°C
	S	P	T	S	P	T		
19	1.754	2.245	1.890	0.950	0.952	0.950	46.30	21.5
20	3.238	3.336	2.997	0.938	0.946	0.932	91.71	22.5
21	3.488	3.174	3.042	0.950	0.952	0.952	135.92	22.5
22	2.314	2.233	2.117	0.950	0.952	0.950	46.30	22.5
23	3.553	3.350	3.081	0.930	0.932	0.926	91.71	22.5
24	2,739	3.421	3.287	0.912	0.914	0.916	135.53	22.5
25	3.874	3.731	3.628	0.900	0.894	0.894	180.77	22.5
26	3.832	-	3.680	0.920	-	0.906	180.77	23.5

Group 3

64.2 w/o glycerol

ν = 10.5 c.s.

Z = 35.66 cm

ρ = 1.1564 gm/cc

C_s^* = 0.75 gm/100 gm soln.

Run #	Dissolution Rate x 10^{-6} gm/sec			Particle diameter cm			Flow rate L/min	Bath Temp °C
	S	P	T	S	P	T		
27	6.007	-	4.735	0.954	-	0.950	46.08	26
28	7.983	5.797	5.878	0.954	0.950	0.952	91.71	26
29	9.572	8.373	8.386	0.940	0.93]	0.934	135.92	26
30	9.607	8.779	8.339	0.922	0.914	0.914	179.91	26
31	5.454	4.803	3.334	0.946	0.936	0.946	46.30	24
32	5.533	6.410	5.392	0.936	0.926	0.934	91.71	24

Group 4

55 w/o glycerol

ν = 6.0 c.s.

Z = 36.27 cm

ρ = 1.1312 gm/cc

C_s^* = 0.62 gm/100 gm soln.

Run #	Dissolution rate x 10^{-6} gm/cc			Particle diameter cm			Flow rate	Bath
	S	P	T	S	P	T	L/min	Temp.°C
33	5.838	5.629	4.632	0.948	0.944	0.944	46.08	24
34	8.743	8.359	7.431	0.936	0.952	0.930	91.71	24
35	7.705	8.570	-	0.942	0.948	-	135.53	24
36	9.221	9.065	8.275	0.922	0.916	0.920	180.77	24
37	6.152	9.635	5.128	0.950	0.946	0.948	46.08	24
38	8.909	8.270	7.675	0.938	0.934	0.936	91.71	24
39	9.742	9.345	-	0.926	0.918	-	135.53	24

Group 5

34 w/o glycerol

ν = 2.5 c.s.

Z = 36.88 cm

ρ = 1.077 gm/cc

C_s^* = 0.43 gm/100 gm soln.

Run #	Dissolution Rate x 10^{-5} gm/sec			Particle diameter cm			Flow rate	Bath
	S	P	T	S	P	T	L/min	Temp.°C
40	1.004	0.971	0.562	0.950	0.948	0.950	46.08	24
41	1.691	1.480	1.361	0.938	0.934	0.936	91.71	23
42	1.561	1.501	1.215	0.946	0.946	0.944	135.53	23
43	1.414	1.488	0.969	0.944	0.934	0.930	180.77	23
44	1.028	0.938	0.927	0.950	0.946	0.914	46.08	23
45	1.804	1.470	-	0.934	0.934	-	91.71	23
46	1.766	1.869	-	0.916	0.918	-	135.53	24
47	1.548	1.532	-	0.910	0.910	-	180.77	23.5

Group 6

Water

ν = 1.c.s.

Z = 39.32 cm

ρ = 1.0 gm/cc

C_s^* = 0.33 gm/100 gm soln.

Run #	Dissolution rate x 10^{-5} gm/sec S	P	T	Particle diameter cm S	P	T	Flow rate L/min	Bath Temp °C
48	2.343	2.154	1.431	0.944	0.942	0.942	46.08	24
49	2.879	2.552	2.233	0.946	0.946	0.942	91.71	24
50	2.949	-	2.207	0.944	-	0.940	135.92	23.5
51	3.513	-	2.922	0.948	-	0.944	180.77	23.5

APPENDIX H

Nomenclature

English letters

A	(1) Constant, Equations (II.8), (II.18), (II.19)
	(2) Area, cm^2, Equation (V.1)
C_1	Constant, Equation (II.10)
C_2	Constant, Equation (II.11)
C_b	Concentration of solute in bulk fluid, gm/cm^3
C_s	Concentration of solute at particle surface, gm/cm^3
C_s^*	Solubility of solute gm solute/gm solution
D	Molecular diffusivity, cm^2/sec
d	Particle diameter, cm
E(k)	Energy spectrum function, cm^2/sec
g	Acceleration of gravity, cm/sec^2
h	Convective heat transfer coefficient, $cal/cm^2.sec\ .°C$
h'	Convective mass transfer coefficient, cm/sec
k	(1) Heat transfer coefficient, cal/cm.sec.°C
	(2) Eddy wavenumber
L	Length scale of primary eddies, cm
n	(1) Eddy frequency, sec^{-1}
	(2) # moles, Equations (V.5) and (V.6)
p	Pressure, $dynes/cm^2$
P_A	Atmospheric pressure, $dynes/cm^2$
Q	Instantaneous turbulence quantity
$\bar{Q}$	Mean turbulence quantity
q	Fluctuating value of turbulence quantity

r	Radius vector, cm
R	Ideal gas constant
T	Temperature, °K
t	time, sec
U,V,W	Instantaneous fluid velocity, cm/sec
u,v,w	Fluctuating values of velocity, cm/sec
V	Velocity vector, cm/sec
x,y,z	Space coordinates
x	Characteristics dimension in dimensionless numbers
X_1,X_2	Exponents, Equations (II.18) and (II.19)
Z	Depth of bath, cm

Dimensionless Numbers

Nu	Nusselt number
Sh	Sherwood number
Pr	Prandtl number
Sc	Schmidt number
Re	Reynold's number
Ko	Kolmogoroff number

Greek Letters

ε	Power input per unit mass of fluid, cm^2/sec^3
η	Length scale of dissipation eddies, cm
μ	Viscosity of fluid, poise
ν	Fluid kinematic viscosity, cm^2/sec
ρ	Fluid density, gm/cm^3
ρ_f	Solution density, gm/cm^3
ρ_p	Particle density, gm/cm^3
ρ_s	Slag density, gm/cm^3
τ	Stress tensor
ϕ	Volume fraction gas entrained in liquid

REFERENCES

1. Brown, J.W., Indian Institute of Metals Symposium on "Recent Developments in Metallurgical Science and Technology," New Delhi, February (1972).

2. Brown, J.W., and R.L. Reddy, Iron Steel Eng., 53 (6), 37-46 (1976).

3. Elliott, J.F., J. Nauman, and K. Sadrnezhaad, "Heating and Melting of DR Pellets in Hot Slag," Proceedings of Third International Iron and Steel Congress, Chicago, Illinois, April 1978.

4. Nauman, J.D., "Analysis of Heat Transfer in Silicate Slags," Sc.D. Thesis, Department of Materials Science and Engineering, Massachusetts Institute of Technology, Cambridge, Massachusetts (1976).

5. Sadrnezhaad, K., "Melting of DR Materials in Steelmaking Slags," Ph.D. thesis, Dept. of Materials Science and Engineering, Massachusetts Institute of Technology, Cambridge, Massachusetts (1979).

6. Salcudean, M., and R.I.L. Guthrie, "Fluid Flow in Filling Ladles," Met. Trans. B., 9B, June 18 (1978).

7. Tarapore, E.D., and J.W. Evans, "Fluid Velocities in Induction Melting Furnaces: Part I Theory and Laboratory Experiments," Met. Trans. B, 7B, September , 343 (1976).

8. Dilawari, A.H., and J. Szekely, "Heat Transfer and Fluid Flow Phenomena in Electroslag Refining," Met. Trans. B, 9B, March, 77 (1978).

9. Dilawari, A.H., J. Szekely, and T.W. Eagar, "Electromagnetically and Thermally Driven Flow Phenomena in Electroslag Welding," Met. Trans. B, 9B, Sept. 371 (1978).

10. Szekely, J., and C.W. Chang, "Turbulent Electromagnetically Driven Flow in Metals Processing. Part I Formulation, Part II Practical Applications," Ironmaking and Steelmaking, 3(3) 181 (1977).

11. Szekely, J., H. J. Wang, and K.M. Kiser, "Flow Pattern Velocity and Turbulence Energy Measurements and Predictions in a Water Model of an Argon-Stirred Ladle," Met. Trans. B, 7B, June, 287, (1976).

12. Hinze, J.O., "Turbulence," "McGraw-Hill Book Company, Inc. (1975).

13. Reynold's, O., Phil. Trans. Royal Soc. of London, 186 Ser. A, 123-164 (1889).

14. Launder, B.E., and D.B. Spalding, "Turbulence Models and Their Application to the Prediction of Internal Flows," Heat and Fluid Flow, 2 (1) 43 (1972).

15. Launder, B.E., and D.B. Spalding, "The Numerical Computation of Turbulent Flows," Computer Methods in Applied Mechanics and Engineering, 3 (2) 269-289 (1974).

16. Harlow, F.H. and J.E. Welch, J. Phys. Fluids, 8, 2182 (1965).

17. Launder, B.E., and D.B. Spalding, "Mathematical Models of Turbulence," Academic Press, London and New York (1972).

18. Batchelor, G.K., "Kolmogoroff's Theory of Locally Isotropic Turbulence," Proc. Camb. Phil. Soc., 43, 533 (1947).

19. Grant, H.L., R.W. Stewart, and A. Moilliet, "Turbulence Spectra from a Tidal Channel," J. Fluid Mech., 12 (2), 241 (1962).

20. Karman, Th. Von., Proc. Natl. Acad. Sci. U.S., 34, 530 (1948).

21. Brian, P.L.T., and H.B. Hales, and T.K. Sherwood, "Transport of Heat and Mass Between Liquids and Spherical Particles in an Agitated Tank," AIChE J., 15(5), 727 (1969).

22. Shinnar, R., and J.M. Church, "Predicting Particle Size in Agitated Dispersions," Ind. Eng. Chem., 52(3), 253 (1960).

23. Kuboi, R., I. Komasawa, and T. Otake, "Behavior of Dispersed Particles in Turbulent Liquid Flow," J. Chem. Eng. (Japan), 5(4), 349 (1972).

24. Froessling, Nils, "Uber die Verdunstung fallender Tropfen," Gerlands Beitr. Geophys., 52, 170 (1938).

25. Ranz, W.E., and W. R. Marshall, JR., "Evaporation From Drops, Part I," Chem. Eng. Progr., 48 (3), 141 (1952).

26. Schlicting, H., "Boundary Layer Theory," 6th. Ed., McGraw-Hill Book Company, New York (1968).

27. Danckwerts, P.V., "Gas Absorption Accompanied by Chemical Reaction," AIChE J., 1(4), 456 (1955).

28. Danckwerts, P.V., "Gas-Liquid Reactions," McGraw-Hill Book Company, New York (1970).

29. Hales, H.B., "Heat and Mass Transfer From Particles Suspended in a Stirred Tank," Sc.D. Thesis, Dept. of Chemical Engineering, Massachusetts Institute of Technology, Cambridge, Massachusetts (1967).

30. Harriott, Peter, "Mass Transfer to Particles: Part I, Suspended in Agitated Tanks," AIChE J., 8(1), 93 (1962).

31. Wadia, P.H., "Mass Transfer from Spheres and Discs in Turbulent Agitated Vessels," Sc.D. Thesis, Dept. of Chemical Engineering, Massachusetts Institute of Technology, Cambridge, Mass. (1967).

32. Woltz, Earl, "The Effect of Gas Agitation on Mass Transfer to Suspended Resin Beads," S.M. Thesis, Dept. of Chem. Eng., Massachusetts Institute of Technology, Cambridge (1973).

33. Levich, V.G., "Physicochemical Hydrodynamics," Translated by Scripta Technica, Inc., Prentice Hall, Inc., Englewood Cliffs, N.J. (1962).

34. Fisher and Porter Catalog # 10A1022

35. International Critical Tables, First Edition, McGraw-Hill, New York (1959).

36. Harriott, Peter, and R.M. Hamilton, "Solid-Liquid mass transfer in turbulent pipe flow," Chem. Eng. Sci., 20, 1073 (1965).

37. Wilke, C.R., and Pin Chang, "Correlation of Diffusion Coefficients in Dilute Solutions," AIChE J., 1(2), 264 (1955).

38. Le Bas, G., "Molecular Volumes of Liquid Chemical Compounds," Longmans, London (1915).

39. Nakanishi, K., T. Fugii, and J. Szekely, "Possible Relationship in Steel Processing Operations," Ironmaking and Steelmaking Quarterly 2(3), 193-8 (1975).

40. Sibree, J.O., "Viscosity of a Froth," Trans. Faraday Soc., 30(3), 325 (1934).

41. Electric Furnace Steelmaking Volume II: Theory and Fundamentals, Physical Chemistry of Steelmaking Committee, Iron and Steel Division, the Metallurgical Society, AIME (1963).

42. Towell, G.D., C.P. Strand, and G.H. Ackerman, "Mixing and Mass Transfer in Large Diameter Bubble Columns," AIChE Symposium Series No.10 (1965).

43. Mickley, H.S., T. K. Sherwood, and C.E. Reed, "Applied Mathematics in Chemical Engineering," Second Edition, McGraw-Hill Book Company, New York (1962).

44. Holman, J.P.p "Experimental Methods for Engineers," McGraw-Hill Book Company, New York (1966).